Shallow-marine depositional sequences in a transgressive mixed siliciclastic-carbonate system: The Early Jurassic Marrat Formation from central Saudi Arabia

Abdullah Al-Mojel, Philippe Razin, Yves-Michel Le Nindre, Guillaume Dera

Shallow-marine depositional sequences in a transgressive mixed siliciclastic-carbonate system: the Early Jurassic Marrat Formation from Central Saudi Arabia

Abdullah Al-Mojel[1, 2], Philippe Razin[2], Yves-Michel Le Nindre[3], Guillaume Dera[4]

[1] Saudi Aramco, Dhahran, Saudi Arabia
[2] ENSEGID-Bordeaux INP, EA4592, 33607 Pessac, France
[3] Ph.D., Dr. Sci. Consulting Geologist, 58 rue Gustave Flaubert - 45100-Orléans - France
[4] GET, Université Paul Sabatier, CNRS UMR 5563, IRD, OMP, 14 Avenue Avenue Edouard Belin, 31400 Toulouse, France

Corresponding author: E-mail: abdullah.mojel@aramco.com Present address: P.O. Box 5093 Dhahran 31311, Saudi Arabia

Keywords: Arabian Platform, Toarcian, Epeiric sea, mixed carbonate-siliciclastic systems, continental-marine transition, transgression, sequence stratigraphy, Marrat Formation

Abstract

A high-resolution sequence-stratigraphic framework is proposed for the Marrat Formation (Early to Middle Toarcian of Saudi Arabia) by presenting new outcrop and shallow core sedimentological data located along a 280 km long N-S transect south of Riyadh and westward subsurface correlations based on gamma-ray wireline logs (200 km Ar Riyadh to Khurais Field). This extended spatial cover allows the identification of a northward thickening of sedimentary successions due to syndepositional differential subsidence. Basically, these successions formed on low-energy falt-topped platform with limited accommodation space in which mainly retrogradational and aggradational stacking patterns were recorded. Overall, the evolution from continental meandering fluvial deposits at the base of the formation to tidal or wave-dominated siliciclastic and carbonate inner-platform deposits indicate a

progressive marine transgression that reached its maximum during the Middle Toarcian *bifrons* Zone. In details, we identify two 3rd-order sequences that onlap southward on to the Triassic−Jurassic unconformity. Higher-energy siliciclastic shoreline facies were deposited in the upper transgressive systems tract of depositional sequences during periods of high accommodation space. The carbonate units consist of platform mud-dominated facies and are well-developed during the maximum marine transgressions of the two Marrat sequences. Continental red shales and fluvial sandstone deposited in a humid and warm environment during the Toarcian *bifrons* Zone (*sublevisioni Subzone*) indicate a higher terrigenous input interrupting the two maximum transgressive sequences. The sequences were likely produced by global sea-level changes but also appear to have been influenced by local climate changes with humid and warm conditions during periods of regression and more arid conditions during transgressions. This study serves as an outcrop analog, provides guidelines for hydrocarbon exploration and improves seismic interpretations. Overall, these new facies analysis, wireline log data, stratigraphic interpretations, and regional correlations contribute to a broader understanding of the Early Jurassic successions of the Arabian Platform.

1 Introduction

The Jurassic formations are one of the most economically important stratigraphic intervals in the world (Powers, 1962; Powers et al., 1966; Powers, 1968; Murris, 1980). Among them, the Marrat Formation (early to middle Toarcian) consists of multiple reservoir units with effective caprocks in the northeast of Saudi Arabia and Kuwait (cf. Alsharhan and Nairn, 1994,

2003; Al-Eidan et al., 2009), as well as possible source rocks reported in Kuwait and Iraq (Abdullah and Connan, 2002; Aqrawi et al., 2010). The sedimentary succession of the Marrat Formation was deposited in the Early Jurassic on a very extensive epeiric tropical Arabian platform (Powers et al., 1966; Murris, 1989) during the first major marine transgression succeeding to the Triassic−Jurassic unconformity (Murris, 1980). The Marrat outcrops are very well exposed in Central Arabia along the base of the Jurassic Jabal Tuwaiq escarpments, which form spectacular west-facing cuestas along a 1000 km axis (Fig. 1).

The outcropping Marrat Formation was previously subdivided into three mapping units based on lithostratigraphic and biostratigraphic correlations (Powers et al., 1966; Powers, 1968; Manivit et al., 1990). However, genetically related depositional sequences, cycle hierarchy, stacking patterns, depositional environment evolution, and effects of syn-depositional tectonic events were not documented in details. Therefore, our approach was to analyses of sections and subsurface gamma-ray logs to generate a robust high-resolution sequence-stratigraphic framework. This study serves as an outcrop analog to the subsurface Marrat Formation of the Arabian Platform and provides guideline for a better understanding of the paleogeographical context and paleoenvironments of the Arabian shelf.

2 Geological Background

2.1 Paleogeographic and tectonic frameworks

The study area was located in the central part of the Arabian Platform, which was an extensive epeiric (> 1000 km) epeiric continental to shallow-

marine platform located in the tropical belt on a passive margin facing the Neo-Tethys Ocean (Murris, 1980) (Fig. 2). The study area was far from the Jurassic shelf margin, which was located hundreds of kilometers to the east, but closer to the exposed Precambrian Shield that was progressively onlapped by the Mesozoic sediments.

Several important tectonic events produced major unconformities across the Arabian Platform during the Mesozoic. Two of these unconformities, respectively Early Jurassic and Late Jurassic-Early Cretaceous in age, delimit the Jurassic Shaqra Group (Vaslet, 1987). The first one, situated at the basal boundary of the Marrat Formation, corresponds to a time gap of approximately 20 Myr having lead to contacts between Triassic and Toarcian deposits. The tectonic control of this unconformity remains poorly understood but could relat to a long period of regional uplift and erosion caused by a tectonic inversion of the Karoo rifting between Madagascar and East Africa (Delvaux, 2001; Baud et al., 2005; Khalifa, 2007; Pöppelreiter et al., 2018) or the early detachment of the Indian Plate from the Africa/Arabia Plate (Grabowski and Norton, 1995). At the top of the Marrat Formation, the Toarcian−Aalenian hiatus corresponds to a major unconformity at the scale of the Arabian Platform, which marks the beginning of the Middle Jurassic Dhruma Formation. This non-deposition event may have resulted from a major sea-level fall of around 75 m (Le Nindre et al., 1990; Al-Husseini, 1997; Jacquin et al., 1998; Simmons et al., 2007; Ogg and Hinnov, 2012; Haq and Al-Qahtani, 2005; Haq, 2018; Simmon and Davies, 2018), large-scale thermal and tectonic uplifts (Le Nindre et al., 2003; Al-Mojel et al., 2018), or a combination of both.

2.2 Stratigraphy and regional depositional history

The Marrat Formation was first defined by Steineke (1937) in an unpublished report but its first formal definition was published by Bramkamp and Steineke (in Arkell, 1952). Its lithostratigraphy was updated by Powers et al. (1966) and Powers (1968) (Fig. 3), in a type section located near the town of Marah in Jabal Kumayt (25° 04' N). A better-exposed reference section in Khashm Ad Dhibi (24° 14' N) was described by Powers and McClure (in Powers et al., 1966) and Manivit et al. (1990).

Powers et al. (1966) divided the formation into three informal units corresponding to the Lower, Middle and Upper Marrat Formation, whose the boundaries were defined using geomorphologic and lithologic criteria clearly visible on the field by the distinction of three three cuestas. The boundaries were slightly revised by Manivit et al. (1990) as follows:

Lower Marrat Unit (47 m thick) is bounded at the base by the Early Jurassic unconformity marked by a stained iron surface on top of the Late Triassic continental Minjur Sandstone. The lithology of the Lower Marrat unit is made up of shale, sandstone and thin dolomitic beds with rare fauna deposited in continental to intertidal-subtidal environments. No biostratigraphic control on the age of this unit is available. These sedimentary facies are clearly distinct of the underlying Triassic Minjur Sandstone characterized by massive amalgamated fluvial braided channels associated with paleosols (Issautier et al., 2012a, b; Stewart et al., 2016; Osman et al., 2018).

Middle Marrat Unit (40 m thick) begins with fossiliferous and bioturbated dolomitic limestone overlain by brick-red shale and siltstone devoid of fossils

record. The top of the unit is marked by calcareous shale with poor fauna content. The depositional setting of this unit ranges from subtidal to intertidal lagoon. The base of the unit is dated by ammonites (*Protogrammoceras* sp.*, Bouleiceras* sp.), which indicate without ambiguity the early Toarcian *serpentinum* Zone (Dubar and Mouterde, 1953; Fig. 3). *Metanoceras* aff. *jurense,* generally assigned to the middle Toarcian in the SE of France (Tintant, 1984), have also been reported but this apparent diachrony could result from earlier appearances on the Arabian Platform followed by a northward migration of this species during the middle Toarcian (Énay et al., 1986, 1987).

Upper Marrat Unit (39 m thick) is a cliff-forming bioturbated lagoonal limestone dated by ammonites (*Nejdia* sp. and *Hildoceras* sp.). The *Nejdia* sp. (likely an evolved genus of *Bouleiceratineae*; Énay et al., 1986, 1987).was discovered in Morocco in the middle Toarcian *bifrons* Zone (*sublevisoni* Subzone), which allows an accurate dating of this unit. Above, this limestone is overlain by a gypsum layer (7 m thick) that has been considered by Powers (1968) as the base of the Middle Jurassic Dhruma Formation. Note that in the subsurface of the Eastern Province of Saudi Arabia, the subsurface Marrat reservoir is recognized as belonging to the upper part of the Marrat Formation (Ayres et al., 1982 in Al-Husseini, 2009 and Manivit et al., 1990).

Overall, the Marrat Formation as a whole was considered as one transgressive – regressive cycle by Le Nindre et al. (1990) with a maximum flooding surface (MFS) at the base of the Middle Marrat (*serpentinum* Zone) corresponding to UAB 4 of Haq et al. (1987) (Fig. 3). Based on a review and interpretation of a single section described by Powers et al. (1966), Powers

158 (1968), Manivit et al. (1990), and Al-Husseini (2009) subdivided the Marrat
159 Formation into two 3rd-order sequences (Marrat Sequence B and A)
160 corresponding to the Arabian Orbital Sequence (AROS; depositional
161 sequence 13.5 and 13.6) scribed to 2.4 Myr eccentricity cycles (Al-Husseini
162 and Matthews, 2008; Al-Husseini, 2009) (Fig. 3). The transgressive system
163 tract (TST) of the Marrat Sequence B consists of a continental shale in the
164 Lower Marrat followed by a maximum flooding interval (MFI) corresponding to
165 the fossiliferous and bioturbated limestone at the base of the Middle Marrat.
166 The highstand coincides with brick-red shale and siltstone of the Middle
167 Marrat. The Marrat sequence A includes the Upper Marrat where the TST and
168 MFS are defined in the basal bioclastic limestone and the khaki shale with the
169 ammonite fauna. The highstand systems tract of sequence A corresponds to
170 the upper gypsum unit (Al-Husseini, 2009).

171 Based on regional correlations of the Jurassic System, Sharland et al.
172 (2001) have placed a maximum flooding surface (MFS J10) in the middle
173 Toarcian Upper Marrat Formation (Fig. 3). On another hand, however, the
174 early Toarcian (*serpentinum* Zone) was selected as the main MFS of the
175 Marrat succession (MFS J10) because the zone has maximal marine faunal
176 diversity (Le Nindre et al., 1990; Kadar et al., 2015; Simmons and Davies,
177 2018).

178 ## 3 Methods

179 Our sequence-stratigraphic study is based on nine detailed logged
180 sections (totaling 600 m in thickness), located along a 280 km N-S transect
181 south of Ar Riyadh. The names of these sections and their locations are
182 shown in Figure 1. One shallow core (DHIBI-1) with gamma-ray logs located

in Khashm Ad Dhibi area near Ar Riyadh is also used in the study. The core only covers the Upper Marrat Formation. The sedimentological data include: mineralogy, grain types, grain size, texture, extended Dunham classification (Dunham, 1962; Embry and Klovan, 1971), sedimentary structure and fossil types and color. The vertical successions and evolution of the depositional environments were analyzed in order to define and interpret sequence stratigraphy.

High-resolution stratigraphic correlations were made using sequence-stratigraphic concepts, physical correlations, and mapping. Applying Walther's Law across the sections was not straight forward, because the platform was aggradational and had limited facies migration. The outcrops are an oblique to depositional strike so may have been more likely to have very gradual lateral facies changes along the transect. Building the depositional model went through a continuous iterative process (Kerans and Tinker, 1997) from one-dimensional cycle stacking analysis and sequence boundary definition to two-dimensional time line correlations and lateral facies organization.

The defined sequences were adopted in gamma-ray logs of nearby subsurface wells in Ar Riyadh and Khurais Fields The sections are complemented with biostratigraphic data of Manivit et al. (1990) and Hughes (2009; unpublished Saudi Aramco internal report of DHIBI-1 micropaleontology). The stratigraphic locations of key biostratigraphic elements (e.g., ammonite faunas) are shown on the cross-section (Fig. 12).

4 Facies and Depositional Environments

Twelve facies or facies associations have been identified from outcrop observations (Figs. 4, 5 and 6 and 7) and are grouped into five depositional

environments based on their common depositional processes. The depositional environments from proximal to distal are: fluvial, coastal plain, high-energy nearshore, mixed carbonate-siliciclastic inner-platform and carbonate inner-platform. Each facies association has been assigned to a sub-depositional environment according to its sedimentological characteristics.

F1: Medium to coarse grained trough/tabular cross-bedded sandstone (braided fluvial system)

This facies is a trough and tabular cross-bedded sandstone, composed of yellowish-orange to light-red, medium- to coarse-grained sandstone; sorting is poor to moderate, with very coarse- to gravel-grade lag deposits occurring primarily in the basal parts of the section, forming lag deposits (Figs, 4A and 9A). This facies occurs in multiple individual sets commonly stacked into cosets, which themselves vary in thickness from 2 to 8 m, with lateral extent of between 7 and 20m.

These trough cross-bedded deposits are of subaqueous origin and represent the migration and accumulation of sandy deposits of sinuous and straight-crested dune-scale bedforms (Miall, 1978; Allen, 1982; Rubin, 1987; Collinson et al., 2006; Al-Masrahy and Mountney, 2015). Sharp boundaries at the bottom of the channel-fill element records a scouring and eroding of the underlying substrate (channel base) by flow circulation in front of the migrating bedforms (Friend et al., 1979; Gibling, 2006).

This unit of sandstone occurs at the base of the Marrat Formation in Wadi Al Jufair (Figs. 8A and 10) and Khashm Ad Dhibi North of latitude 23º 50’ N and in the Middle Marrat unit in Wadi Birk and Fara’id Al Ahmar (Fig. 12). The

sandstone overlies the Triassic−Jurassic unconformity in the northern sections and are intercalated with barren red shales (F4) within the Middle Marrat unit.

F2: Inclined argillaceous stratified sandstone (fluvial meandering channel)

This facies association is present in 0.5 to 5 m thick sharp-based lenticular bodies intercalated with barren red shales within the Middle Marrat unit. Lenticular, fine to medium grained sandstone units form the lower part of a channel-fill sequence. The rest of the sequence is made of a fining-up alternation of pale yellowish fine-grained sandstone and mud. (Figs. 5A, B, C, and 9C; Table 1). The dip of these inclined stratifications is highly variable in the successive stacked sequences, indicating lateral accretion processes in point-bar deposits within low-energy meandering channels (cf. Thomas et al., 1987).

These facies represent the deposition under the influence of upper flow-regime conditions, in confined channel flow, during the final stage of channel fill and abandonment (Miall, 1977, 1996; Bridge, 2006); the presence of clear fining up and the high percentage of mud toward the top of the succession suggests the deposition under the influence of upper flow-regime conditions, in confined channel flow, meandering fluvial system (Olsen, 1987; Miall, 1996).

F3: Ripple cross-laminated sandstone (fluvial overbank)

This lithofacies is characterized dominantly by cross-laminated silty sandstone that is light red, very fine-grained, and which occasionally

possesses dark mud drapes on some lamination surfaces. This facies is also characterized in places by ripple-form stratification. Ripple forms may occur in trains (Figs. 5D and E). This facies occurs in the upper parts of sets as packages of ripple cross-lamination and ripple-form strata 0.2 to 0.5 m thick. Ripple forms are especially well developed on upper bedding surfaces of sets. This facies is commonly closely associated with horizontally laminated sandstone facies.

This facies accumulated in subaqueous conditions (fluvial); and represents the unidirectional migration of small-scale ripple forms during waning flow regimes, this facies formed within either the upper part of the fluvial channel-fill or in non-channelized fluvial settings, i.e. overbank and natural levee deposits (McKee, 1966; Stear, 1985), under generally a slow and shallow water flow (Nichols, 2009; Banham and Mountney, 2014). This facies found in the Middle Marrat unit at the same stratigraphic level as the previous meandering channel facies association.

F4: Red thinly laminated mudstone (flood-plain/lake)

In the northern part of the studied transect, the Middle Marrat member is mainly composed of 3 to 27 m thick homogeneous red laminated mudstone units, that are commonly laterally extensive, extending for 280 km across the entire section of the fluvial part of the outcrop. The basal and upper contacts of these units are gradational and marked by a transitional change from red to grayish green mud with about 10% of thin siltstone lamina (Fig. 5F; Table 1), this color changes may reflect weakly developed pedoturbation or fluid bleaching (Wright, 1986). The mudstone lamination indicates the deposition from very weak flow or standing water (Fisher et al., 2008). X-ray diffraction

282 analysis shows that the red shale is mainly composed by kaolinite with minor
283 amounts of illite and feldspar (Abed, 1979). The red color of clays is due to
284 the presence of hematite. The muddy intervals of flood plain origins in this
285 area are generally barren (Powers et al., 1966) and their association with
286 fluvial channel-fills and overbank deposits suggest a broad alluvial flood-plain
287 environment with probable ephemeral lake development recorded by the thin
288 silty lamination in some intervals (Willis and Behrensmeyer, 1994, Church, M.
289 2006; Fig. 5F). The high amounts of kaolinite and hematite suggest a tropical
290 equatorial paleoenvironment with very humid condition favoring chemical
291 weathering processes as laterization (Chamley, 1989; Dera et al., 2009).

292 **F5: Mottled red shale (paleosol)**

293 This facies is represented by 0.5 to 1.5 m thick muddy units and are
294 commonly capped by reddish-brown crust (oxidized). The facies mainly
295 consists of clay and silt enriched in kaolinite, hematite, and various elements
296 (Ti, Zr, Nb, and Y) indicating considerable alteration of sediment accumulation
297 under tropical conditions (Abed 1979; Kraus, 1999).

298 The muddy intervals are mottled, orange, pink and red, with root traces
299 (Fig. 5G; Table 1). This facies is associated with fluvial channel-fill deposits
300 (F2) representing the final stage of deposition, channel abondenment (Miall,
301 1996). This facies occurs in the Middle Marrat member and especially in the
302 southern outcrops that correspond to the more proximal setting. The color
303 contrasts and mottling could indicate organic oxidation in paleosol deposits
304 (Wright, 1986; Collinson, 1996; Kraus, 1999; Hatano and Yoshida, 2017).

F6: Mottled bluish green shale with interbedded mudstone and sandstone (mud-flat/coastal-plain)

The facies association occurs as 0.5 to 17 m thick tabular units. It mainly consists of bluish green shales mottled red and brown (Fig. 6A; Table 1). The facies association consists of clay, silt and fine to medium sand. From Khashm Ad Dhibi core (DHIBI-1), the shale is reddish brown with fissile parting. The facies association is present in the Lower and Upper Marrat members. In the Lower Marrat member, the shale is barren and associated with thin orange dolomite, stromatolitic lime-mudstone (Fig. 6B) and mud-draped cross-bedded sandstone. The associated sandstone and lime-mudstone exhibit desiccation mudcracks. In the Upper Marrat member, the shale is interbedded with channelized cross-bedded sandstone (F8) of tidal origin. The facies association is deposited on low-energy mud flats in a coastal-plain setting.

F7: Bioturbated heterolithic siltstone and sandstone (mixed-flat/coastal-plain)

These facies association consists of tabular units 0.5 to 2 m thick coarsening-upward gradational bases and sharp tops. The facies association consists of siltstone to medium-grained sandstone. They are intensely bioturbated mainly by horizontal burrows (Fig. 6C; Table 1), which mixed the silt and sand. The facies association is developed in the Upper Marrat member intercalated with the bluish green shale (F6) deposited in a tidal flat environment. These facies usually grade up into tidal and/or wave influenced massive sandstone (F8 to F10), which suggests a mixed tidal flat/coastal plain

329 depositional setting transitional between the wave-dominated shoreface and
330 the tide-dominated mud flats.

331 **F8: Cross-bedded sandstone with mud drapes (tidal creeks)**

332 This facies occurs in 0.5 to 1.5 m thick lenticular bodies bounded by an
333 erosional surface at the base and commonly sharp, iron stained and
334 bioturbated surface at the top. The facies is made up of medium-grained
335 sandstone including some plant debris. The deposit is characterized by
336 tabular cross-bedding and mud-draped current ripples indicating tidal
337 influence (Figs. 6D and E; Table 1). The cross-sets, in some cases, show
338 sigmoidal foresets with mud-drapes. This facies is well developed only in the
339 Upper Marrat member interbedded mainly with the mottled bluish green shale
340 (F6) and locally with bioturbated heterolithic silty sandstone (F7). The facies is
341 interpreted to be deposited in tidal creeks draining a wide low-energy lower
342 coastal plain (cf. Ginsburg, 1975; Weimer et al., 1982). The tidal influence is
343 suggested by the mud-draped current ripples and sigmoidal foresets (cf.
344 Tankard and Hobday, 1977; Banerjee, 1991).

345 **F9: *Skolithos*-bearing bidirectional cross-bedded sandstone (tidal**
346 **bars and channels)**

347 This facies forms 0.5 to 1.5 m thick tabular to lenticular units with sharp
348 bases, and iron-stained bioturbated tops. The facies consists of medium-
349 grained sandstone including plant debris and displaying bidirectional
350 megaripple cross-bedding of tidal origin. The facies is highly bioturbated with
351 abundant *Skolithos* sp. trace-fossils (Fig. 6F; Table 1). It occurs in the topmost
352 of the Marrat Formation on top of the paleosols (F5), bluish green shale (F6),

bioturbated heterolithic silty sandstone (F7) and wave-influenced sandstone (F10). The facies is interpreted to be deposited in tidal bars and channels in a nearshore environment. (cf. Fery, 1975; McIlroy, 2004; Miller, 2007; Gerard and Bormley, 2008).

F10: Swaley cross-stratified sandstone (shoreface)

The facies occurs as 1 to 2 m thick tabular units having sharp scoured bases and bioturbated tops (Fig. 6G, H; Table 1). The facies consists of medium-grained sandstone including intraclastic reworked pebbles and are characterized by swaley cross stratification (SCS; Leckie and Walker, 1982) and some hummocky cross-stratifications (HCS; Harms et al., 1975; Leckie and Walker, 1982). Sometimes, this facies grades up to bidirectional cross-bedded tidal sandstone (F9). Otherwise, the SCS sandstones are sometimes sharply overlain by tidal creek sandy deposits (F8) bioturbated heterolithic silty sandstone (F7) or grayish green shale (F11). This facies can be interpreted as a wave and storm dominated shoreface sands (cf. Dumas and Arnott, 2006).

F11: Grayish green calcareous shale (shale dominated inner-platform)

The facies appears as 1 to 4 m thick olive gray to greenish gray units. They are made up of terrigenous clay and admixed carbonates (Fig. 7A; Table 2). The shales are brittle, flaggy and slabby. In core, the calcareous shale shows thin laminations, rare *Chondrites* burrows and reworked mollusk debris (Fig. 10). The calcareous shale contains gastropods, bivalves and locally ammonites (Manivit et al., 1990). The calcareous shale is mainly

interbedded with bioturbated quartzose lime-mudstone and mottled bluish green shale (F6), which suggest an inner platform setting close to the continental to coastal plain terrigenous source. The rare *Chondrites* burrows, rare macrofauna and the thinly laminated sedimentary structure suggest restricted conditions that could result from a sub-oxic bottom water (Bromley and Ekdale, 1984). The driving control of the restriction in such shallow water is probably the high coastal nutrient influx and the surface runoff which could cause density stratification that prevented vertical circulation of bottom water (Bottjer et al., 1986 in Read, 1989; Rabalais et al.,1991; Lukasik et al., 2000).

F12: Argillaceous nodular peloidal mudstone/wackestone (mixed inner-platform)

This facies occurs in 1 to 3 m thick tabular units, which are commonly bounded by sharp base and top. The base of the units are often marked by reworked intraclasts and skeletal fragments. The facies is made up of slightly argillaceous muddy carbonate facies including pellets, peloids, intraclasts, skeletal fragments and locally 20 to 50% fine to medium quartz grains. The fossil assemblage consists of ammonites, bivalves, gastropods, echinoid, brachiopods and agglutinated foraminifera such as *Ammodiscus* sp. (Manivit et al., 1990; Hughes, 2009; unpublished report DHIBI-1 micropaleontology). The facies exhibits a nodular sedimentary structure (Fig. 7B; Table 2), argillaceous wispy lamination in core sample and thin horizontal burrows 5 mm wide (Fig. 7C). The facies is present in the upper part of the Lower Marrat and Upper Marrat units. The facies is interpreted to be deposited in a low-energy mixed inner-platform with limited siliciclastic influx. As they are localized between dark-colored calcareous shale (F11) and light-colored

bioturbated lime-mudstone (F13), it is interpreted to record the transition from less-oxygenated to well-oxygenated conditions.

F13: Bioturbated peloidal wackestone/mudstone (carbonate inner-platform)

This facies consists of 1 to 3 m thick tabular units, with a transitional base and bioturbated firmground at the top (Figs. 7C and D; Table 2). The facies is made up of very fine pelletal peloidal grains. The facies is highly bioturbated with branched vertical burrows (*Thalassinoides*) that tend to homogenize the sediments and destroy the primary sedimentary structures. Moreover, they may have argillaceous wispy solution seams and rare nodular sedimentary structures. The fossil assemblage consists of echinoids, brachiopods, molluscs (*Inoceramus* sp. fragments), and benthic foraminifera (*Siphovalvulina variabilis*, *Valvulina* sp., *Haplophragmoides* ssp., *Ammobaculites* sp., *Textulariopsis* sp.) (Fig. 10; Hughes, 2009; unpublished report). The facies is interbedded with the slightly argillaceous horizontal limestone (F12). It is only present in the northern two sections (Fig. 12).

The light color of this facies and the intense bioturbation suggest a well-oxygenated environment and a relative normal marine condition (Wilson and Jordan, 1983; Galli, 1993; Khetani and Read, 2002). The foraminiferal association is considered as the most open-marine biofacies in generally restricted low-oxygenated environment (Hughes, 2009; unpublished report).

5 Depositional Model

The spatial distribution and the lateral relationships of the facies are illustrated in an idealized depositional model (Fig. 11). This depositional

model is built using the sedimentological characteristics, vertical facies successions in individual logs (e.g., Figs. 9 and 10) but also the lateral organization of the facies given by the correlation established along a 280 km long transect (Fig. 12).

The depositional model represents a continental to inner-platform shallow-marine depositional settings with two depositional domains including a siliciclastic-prone proximal domain and carbonate-prone distal domain. The siliciclastic proximal domain consists of alluvial system and wide shale-prone coastal plain to inner-platform environment with limited fluvial dynamics. They are characterized by a low-energy tidal flat and occasional wave-dominated environment. In such flat inner-platform, higher-energy deposits are represented by narrow facies belt of SCS sandstone (F10) resulting from repeated marine transgressive events (cf. Wilson, 1975). The higher energy nearshore environments were better developed during periods of high accommodation rates (Late TST and MFS) in which higher water-depth favor wave propagation and stronger tidal currents. The carbonate-dominated distal domain consists of shale-prone and mud carbonate-prone inner-platform. The shale-prone inner-platform is in a relatively proximal setting influenced by siliciclastic influx, whereas carbonate-prone inner-platform representing the most open-marine environment. The carbonate inner-platform deposits (Fig. 10) show no evidence of wave-base or mid-ramp high-energy facies in a classical sense. High-energy carbonate facies in such flat inner-platform settings appears at base of the HFSs (Fig., 10) considered as transgressive reworked sediments. Interestingly, these basal grainy facies coincide with the appearance of the most open-marine biofacies (foraminifera) in generally

restricted low-oxygenated environment, which confirm that the waves are transgressive related process. The bathymetry of the Marrat depositional environments was probably never more than a few meters based on the occurrence of time-equivalent fluvial facies to the south.

The objective of this idealized depositional model is to give a relative position to each identified facies and does not indicate synchronous facies. This is because the sedimentary systems kept changing through time and evolved within a depositional sequence. For example, siliciclastic facies are more dominant during early transgressive periods, whereas, carbonates develop widely during late transgression and highstand periods.

6 Sequence Stratigraphy

Correlations between nine sedimentological sections in the Marrat Formation result in a regional transect oriented in an oblique-dip direction. The base of the transect is picked at the Triassic−Jurassic unconformity, which is a sharp erosional surface at the top of the fluvial Minjur Sandstone. The top of the cross section is picked at the top of the Marrat Formation, which is the Early–Middle Jurassic unconformity. The unconformity is overlain by local evaporites to the north and laterally continuous ferruginous oolite to the south. The Middle Marrat continental red unit shows continuous extension along the outcrops. The lateral facies changes in the shallow-marine environment indicating an apparent S-N dip direction of the depositional system.

The facies distribution along this regional transect shows that the Marrat Formation comprises two composite sequences (MCS1 and MCS2). Each in turn consists of five high-frequency sequences (HFS1 to HFS5). The first

composite sequence (MCS1) includes the Lower Marrat and a part of the Middle Marrat unit and the second (MCS2) includes a part of the Middle Marrat and the Upper Marrat units (Fig. 12). The MFS of MCS1 coincide with the MFS of sequence B of Al-Husseini (2009), MFS J10 of Kadar et al. (2015) and Simmons and Davies (2018). The top sequence boundary of MCS1 is slightly lower than Al-Husseini's (2009) sequence boundary.

The composite sequences onlap southward onto the Triassic−Jurassic unconformity. The regional geometry of these continental to shallow-marine deposits show a clear differential subsidence along the transect with the north subsiding faster than the south. This differential subsidence appears rather homogeneous except between Wadi Al Jufayr and Faridat Balum where a strong increase of the subsidence rate is recorded by wedging stratal geometries.

The main maximum marine transgression is in the *bifrons* Zone near the top of the Marrat Formation (MCS2). There is no evidence of progradational stacking patterns or low-stand deposits as most of the accommodation space remained full throughout deposition. The top of the Marrat Formation that corresponds to the long-lived Aalenian hiatus and probable subaerial exposure does not exhibit any fluvial incisions, indicating the lack of any efficient fluvial system and probably a very flat topography at that time.

In the reference section (Khashm Ad Dhibi), the vertical facies successions of the Marrat composite sequences are both beginning by basal transgressive fluvial deposits characterized by a set of individual fluvial channels interfingering with red siltstone and shale. The fluvial deposits grade upward to mixed carbonate-siliciclastic coastal-plain and inner-platform facies

501 (Figs. 8 and 9). The maximum marine transgressions of these composite
502 sequences are interpreted in the clean bioturbated limestone inner-platform
503 facies (F13; Figs. 8, 9 and 10). These MCS are clearly asymmetric in
504 thickness with a thick transgressive unit and much thinner regressive one.
505 This asymmetric pattern is related to very shallow marine conditions in the
506 inner platform where sediments are only preserved during the stage of
507 increasing accommodation space,

508 **6.1 Marrat composite sequence 1 (MCS1)**

509 Marrat composite sequence MCS1 is 85 m thick in the northern area
510 (Khashm Ad Dhibi) and thins out and pinches out at the most southern
511 section. The basal sequence boundary is the Triassic−Jurassic unconformity
512 marked by a very sharp contact (Fig. 8A), paleosol and iron-crust surfaces on
513 top of the Minjur Sandstone fluvial deposits. In the most complete sections,
514 the early TST (0 to 40 m thick) consists of a basal fluvial sandstone unit (F1)
515 overlain by barren bluish green shale coastal-plain facies (F6). It is made up
516 of at least three high-frequency sequences (HFS1 to 3) characterized by
517 asymmetrical transgressive cycles with thick basal shale deposits. HFS1 is
518 capped by a thin cross-bedded sandstone unit displaying mud-drapes and
519 mudcracks. HFS 2 and 3 are capped by thin stromatolitic lime-mudstone and
520 dolomite bed. These HFSs are aggradational at the base of the northern two
521 sections and pinch-out completely between Wadi Al Jufair and Faridat Balum
522 sections.

523 The late TST (0 to 23 m thick) of MCS1 is dominated by mixed carbonate-
524 siliciclastic inner-platform facies and made up of at least two high-frequency
525 sequences (HFS4 and part of HFS5). It starts with a thin fluvial sandstone bed

grading upward to brown shale, representing coastal-plain (F6) and to inner-platform quartzose nodular lime-mudstone (F11) interbedded with green calcareous shale (F12). The calcareous shale and the quartzose lime-mudstone grade updip into shoreface swaley cross-stratified sandstones (F10; Khashm Khalta and Khashm Disman). These shoreface sandstones form narrow high-energy wave dominated facies belt that appear during periods of relatively high accommodation rate. Further updip, there are also several fluvial units between Khashm Al Khalta and Fara'id Al Ahmar indicating a transition to nonmarine facies that are time-equivalent to the marine facies farther north. In the northern sections, the MFS is marked by inner-platform highly bioturbated peloidal lime-mudstone (F13). South of Faridat Balum section, these pure carbonate deposits grades to mixed siliciclastic-dolomitic then argillaceous facies that finally onlap directly on the Minjur Formation in Fara'id Al Ahmar section. So, even though marine conditions occurred to the north, there was still subaerial exposure to the south.

The HST of the MCS1 has a progressively lower carbonate content and consists of coastal-plain green shale (F6) that progressively grades upward into flood-plain/lake thin laminated red shales (F4) of the Middle Marrat unit. These highstand red shales form an aggradational and tabular 15 to 20 m thick unit in the northern area. It pinches out gradually southward. The sequence boundary is placed at the base of the fluvial channel-fill sandstones that are locally intercalated with the red shales.

6.2 Marrat composite sequence 2 (MCS2)

The MCS2 is 50 m thick in the northern area (Khashm Ad Dhibi) and thins to 4 m thick to the south. The basal sequence boundary is placed at the base of the fluvial channels in the Middle Marrat. The early TST is marked by retrogradational stacking pattern made up of at least three high-frequency sequences (HFS1 to HFS3) onlapping towards the south. They are characterized by shale dominated low-energy fluvial, coastal plain and inner-platform facies. The high-resolution stratigraphic correlations show that the more proximal coarse-grained and cross-stratified fluvial facies are dominant in Wadi Birk – Fara'id Al Ahmar, and secondarily in K. Al Khalta areas but are absent in the southernmost part of the transect. They grade to more distal shaly deposits northward and to lower energy fluvial deposits southward in the area of minimum accommodation, but no fluvial incisions are noticed. This observation suggests that the orientation of the fluvial systems is oblique to the studied transect with a probable west-east component.

In detail, HFS1 is entirely made up of fluvial sandstone and shale deposits up to 25 m thick overlain in the northern section by transgressive thin reworked peloidal skeletal packstone of HFS2 (Fig. 10). HFS2 is a 9 m thick symmetrical cycle and is made up of grayish green calcareous shale (F11) with thin reworked skeletal intraclastic rarely bioturbated wackestones (F12) (Fig. 10). HFS2 shows an increase in quartz content updip grading into fluvial red shale (F3/F4) and point-bar sandstone (F2). HFS3, 2.5 to 5.5 m thick, begins with sharp-based skeletal wackestone fining upward to weakly bioturbated argillaceous lime-mudstone (F12) and capped by coastal-plain reddish brown shale (F6) (Fig. 10). This HFS3 grades updip into well-

developed tidal cross-bedded sandstone (F9) and further to the south into fluvial sandstone and associated red shales.

The late TST is made up of two backstepping HFSs (HFS4 and lower part of HFS5). From north to south, the depositional system consists of several facies belts: a mixed carbonate-siliciclastic (F11/F12), a narrow and localized wave-dominated nearshore sandstone belt (F10), an inner platform to coastal plain shale-dominated environment with tidal channel sandstones (F6 to F9) and alluvial red shales and heterolithic point-bar deposits (F2 to F4). HFS4 is a symmetrical transgressive-regressive sequence up to 6 m thick (Fig. 10). It begins with a sharp base, overlain by argillaceous transgressive reworked skeletal intraclastic wackestone (F12; Khashm Ad Dhibi) or scour-based swaley cross-stratified sandstone (F10; Khashm Khalta). At the base of HFS4, ammonites dated as middle Toarcian (*bifrons* Zone) were found in calcareous shale inner-platform facies in Khashm Ad Dhibi (Manivit et al., 1990). The calcareous shale (F11) grades upward to slightly argillaceous lime-mudstone (F12) interpreted as the MFS of this high frequency sequence. The argillaceous lime-mudstone (F12) progressively changes to coastal-plain green shale (F6) and tidal sandstone (F8) without passing through high-energy shoreface deposits. In the most southern sections, HFS4 consists of fluvial sandstone capped by paleosol. HFS5 is a symmetrical transgressive-regressive cycle ranging from 2.5 to 7 m in thickness. From north to south, it begins with slightly argillaceous wackestone/packstone (F12; Khashm Ad Dhibi), sharp-based wave dominated sandstone (F10; Khashm Khalta) or tidal point-bar sandstone (F8; Khashm Disman).

598 Upper HFS5 (HST of MCS2) is very thin (< 5 m). It is dominated by
599 shallow-marine carbonate and sandstone with little shale content. In the
600 northern section (Khashm Ad Dhibi), it is made up of thinning-up slightly
601 argillaceous carbonate parasequences with some *Chondrites* burrows and
602 capped by a hardground surface (Fig. 10). In a more proximal position, it is
603 marked by a minor progradation of the nearshore sandstone belt (F10,
604 Khashm Khalta to Faridat Balum; Fig. 12). Then, the facies succession shows
605 a decrease of the wave influence and a relative increase of tidal processes
606 with the occurrence of bidirectional cross-bedded sandstone (Faridat Balum,
607 Khashm Khalta and Khashm Disman) and *Skolithos* sandstone with plant
608 debris (F9). The HST wedge out to the south where it is represented by iron-
609 stained surfaces.

610 The maximum transgression of the whole Marrat cycle corresponds to
611 MFS of the MCS2. In Khashm Ad Dhibi to the north, it is marked by a
612 relatively thick highly-bioturbated pelletal lime-mudstone considered as a
613 shallow-marine low-energy inner carbonate platform facies, the most distal
614 marine facies of the entire Marrat Formation (Fig. 10). It grades updip to
615 calcareous shale (F11; Wadi Al Jufayr), then to relatively higher energy sand
616 dominated shoreface to backshore/tidal flat deposits. The shoreface is
617 represented by scour-based intraclastic swaley cross-stratified sandstone
618 (F10, Faridat Balum). In a more proximal position, tidal-influenced sandstone
619 and heterolithic facies are deposited in a backshore to tidal flat environment
620 (F7 to F9; Khashm Disman to Fara'id Al Ahmar).

621 The upper sequence boundary of MCS2 is a hardground surface overlain
622 by 7 m of evaporites in the Khashm Ad Dhibi section to the north (Fig. 10).

Lithostratigraphically, these evaporites were considered as part of the Marrat Formation (Manivit et al., 1990). However, they are not genetically related to the Marrat depositional system but to the Dhruma sequence (Al-Mojel, 2017) consistent with Powers (1968). This evaporitic unit is restricted to the most subsided area in the north (Khashm Ad Dhibi) and is absent to the south. From Faridat Balum to Abu Al Jiwar (more than 200 km long), the top Marrat unconformity is overlain by a silty ferruginous oolite horizon up to 0.5 to 5 m thick lying on top of the thin but highly continuous HFS5 with no evidence of major erosion. This stratal continuity below and above the Early-Middle Jurassic unconformity confirms the very flat topography and high stability of this part of the Arabian Platform during the Aalenian period.

7 Discussion

7.1 Inner platform development

During the Early Jurassic, the Arabian Platform underwent gentle differential subsidence. The continuous and slight subsidence controlled the thickness of the strata as well as lateral facies distribution (Fig. 12). Thus, the platform aggraded as a response to the rotational differential subsidence and stacked thick shallow-marine deposits wedging and thickening toward the depocenter.

At the onset of the Jurassic transgression, the Arabian Platform was a very flat low-energy, shallow-marine homoclinal ramp as attested by our stratigraphic transects (Fig. 12 and 13). A minor slope of 0.1 m/km is calculated from the top of Marrat Formation from the shoreline (Faridat Balum) to the most distal section (Khashm Ad Dhibi) in a corrected dip

direction, assuming NE dip. This flat-topped profile is mainly related to the overall geodynamic setting, where the studied domain is located in the inner part of a very wide epeiric platform on the Neo-Tethys passive margin with stable tectonic context. The limited accommodation rate is compensated and filled by siliciclastic supply and carbonate production. The very flat depositional profile is also indicated by the large area of tidal influence in the siliciclastic coastal plain and the meandering pattern of the fluvial system of the middle Marrat unit. In the subsurface, the Marrat reservoir in Kuwait consists of sheet and shoal of grainstones that are underlain and overlain by extensive sabkha and tidal flats deposits (Al-Eidan et al., 2009). The lower sabkha and tidal flat units in Kuwait could correlate to the lower Marrat of Khashm Ad Dhibi that is dominated with tidal-flat stromatolite laminated mudstone. The upper sabkha and tidal flat units in Kuwait could tie to the crinkly laminated evaporite at the base Dhruma sequence (Fig. 13). These extensive sabkha and tidal flats attest a predominantly flat-topped platform during Marrat deposition. Moreover, west of the Qatar Arch in the Rub' Al-Khali and Oman, the Marrat Formation has two distinct carbonate units that extend for 500 km across the platform (Fig. 13; Stewart et al., 2016). The lack of evidence of major channel incisions or prograding clinoforms during relative sea-level fall or still stand can be also considered as a consequence of the very low gradient with probably limited sea level changes in what were likely greenhouse conditions (Summerfield, 1985; in Blum and Törnqvist, 2000). Moreover, the lack of high-energy sediment transport processes and the low sediment production, both carbonate and siliciclastic in proximal setting, led for very low gradient depositional profile (0 to 0.4°) (Williams et al., 2011).

The Marrat Formation is characterized by low-energy mud-dominated coastal plain to inner-platform setting with limited fluvial input. Higher-energy depositional settings only occur during late TST and MFS when paleobathymetry is enough to allow wave propagation in the inner-platform setting. The coastal plain at the base of MCS1 is very low-energy marked by barren shale with thin stromatolites lime-mudstone (Fig. 10). The high-energy wave influenced siliciclastic facies (F10) appears during late transgression as short-lived wave reworking sandstone. Similarly, the MCS2 begins with low-energy shale and lime-mudstone that progressively evolved to higher-energy tidal creeks and shoreface sandstone. Generally, the tidal creeks require higher-energy to transport the sediments and to form channel-beds (Davis, 2012). Moreover, high-energy deposits resulted from repeated marine transgressive events in this kind of flat-topped wide platform with slow sedimentation rate (Wilson, 1975). During the HST, the influence of the wave decreased upward and, instead, tidal influence is preserved in sandflat with prominent bidirectional cross-bedding and *Skolithos* sandstone (most top of MCS2).

The carbonates of the Marrat Formation are low-energy mud-dominated facies with reworked skeletal intraclastic wackestone/packstone (Fig. 9). They show very consistent flat tabular aggrading units that pinch out to the south. (Fig. 12). The carbonate production in such mixed system is weak with common interbedded shales and hardground/firmgrounds early-cemented surfaces near the base of the sequences (Fig. 10; HFS2, 3 and 4 of MCS2). This low carbonate production is probably controlled by the overall restricted inner-platform condition and poorly oxygenated bottom water due to the fresh-

water runoff. The carbonates are well developed during maximum marine transgression (Late TST and MFS; TST of HFS5 of MCS1 and MCS2) in well-oxygenated inner-platform setting.

This depositional sequence model suggested here has some sort of agreement with a new sequence stratigraphic model proposed by Horbury (2018) for Triassic to Middle Jurassic of the NW Arabian Platform. Horbury's (2018) model is designed for restricted inner-platform depositional system, unlike the classical carbonate sequence stratigraphic models (Sarg, 1988; Sarg et al., 1999) that were dedicated for open marine and shelf-margin condition. Horbury (2018) placed fluvial deposits and restricted lithofacies (e.g., interbedded anhydrite and dolomite, marginal marine shale) in lowstand system tracts (LST) and early transgressive systems tract (early TST), whereas higher-energy carbonates and deep-water shale are well developed later in TST and MFS. A prograding clinoforms with open-marine conditions were placed in highstand systems tract (HST). These late-TST high-energy carbonate and the highstand prograding clinoforms can be observed in Kuwait (Al-Eidan et al., 2009) and probably in Abu Dhabi (Al-Sharhan et al., 2014), but not in the Marrat outcrop as it is considered a restricted inner-platform setting. This implies that the Arabian Platform is a unique extensive shelf that has no analog counterpart whether modern or ancient.

7.2 Controlling factors of the Toarcian Marrat Formation

7.2.1 Tectonics and subsidence

The Marrat Formation records an overall relative sea-level rise after the tectonic related Triassic−Jurassic unconformity, which is in agreement with a

global eustatic rise during this period (Haq, 2018). Differential subsidence of the Arabian Platform at this location promoted the onlapping geometries on the underlying Minjur unconformity (Kuwait and Oman; Clarke, 1988; Yousif and Nouman, 1997; Stewart et al., 2016). The effect of the subsidence is very clearly demonstrated along the transect by the complete wedging and onlap of the succession from north to the south. The maximum accumulation rate of the Marrat Formation, calculated by dividing the total thickness of the formation by the 3.5 Myr duration of the *serpentinum* Zone and *bifrons* Zone (Gradstein et al., 2012) is 3.9 cm/kyr (Khashm Ad Dhibi). This falls within the lower range of passive margins accumulation rate (few centimeters to 10 cm/kyr; Bott, 1992). The low accumulation rates of the non-marine and coastal-plain siliciclastic sections are below this range (e.g., Khashm Khalta 1.83 cm/kyr, W. Birk 1.2 cm/kyr, K. Abu Al Jiwar 0.13 cm/kyr). Most of the time, these wedging geometries and the northwards increase of subsidence are very progressive all along the transect with an average of 35 m/100 km. However, at the beginning of the Marrat transgression (MCS1), the subsidence rate becomes rapidly higher between Faridat Balum and Wadi Al Jufayr (65 m/100 km). This suggests a local tectonic control of the subsidence in this area, which could have favored the initiation of the Toarcian onlap in this domain.

The Ar Rayn Terrane (approximately between 24° N to 25° 20’ N) was a tectonically active structure and played a significant role in the basin configuration of the study area. The Ar Rayn Terrane during the late Triassic was probably uplifted and was eroded (Le Nindre et al., 2003). During the Jurassic, the Ar Rayn Terrane subsided rapidly, which probably caused the

depocenter axis of the Early and Middle Jurassic outcrop (cf. Fig. 72 of Manivit et al., 1990; Fig. 3 of Fischer et al., 2001). The lack of real unconformity (i.e., toplap/onlap geometries) along the Early-Middle Jurassic unconformity, which correspond to a very long period (late Toarcian-Aalenian) attests very high stability of this domain during the Jurassic long-term transgression.

7.2.2 Eustatic controls

In our study, the main MFS of the whole Marrat succession is within the middle Toarcian (*bifrons* Zone) shown by the maximum landward extension of the Upper Marrat carbonate unit. This is in concordance with the Arabian Plate MFS J10 (Fig. 14; Sharland et al., 2001), which coincides with a positive $d^{13}C$ peak interpreted by Al-Mojel et al. (2018) as a sign of important marine productivity levels favored by a high sea-level. Consistently, the *bifrons* Zone marks the interval of the highest global sea-level rise during the Early Jurassic (Haq et al., 1988, Haq, 2018) and the major MFS of the NW Tethys in the European domain (Hardenbol et al., 1998) and drowning event in the Mediterranean domain (Jenkyns et al., 1985; Crevello, 1990). Subordinate MFS (MFS J09) have to be placed in the early Toarcian (*serpentinum* Zone) in the highly bioturbated carbonate interval of the Lower Marrat unit. Caution should be used if attempting to relate normal-marine depositions and/or high faunal diversity interval as a main eustatic MFS without seeing the geometrical stacking patterns. In such mixed carbonate-siliciclastic platform, true MFS is difficult to recognize without a regional context (Davies et al., 2002). During certain marine transgression, outer-platform with normal-marine depositional condition can jump in inner-platform setting especially after

environmental related carbonate decline (Hunt and Tucker, 1993). Thus, having a highly bioturbated carbonate interval with maximum faunal diversity in the first marine transgression event (Serpentinum Zone) could be a consequence of the major early Toarcian extinction (Fig. 15) and not just a result of maximum eustatic rise. The biodiversity can also be controlled by the physiography of the carbonate platform (e.g., width, inclination, occurrence of a barrier) which is not the same (at least the width) between MCS1 and MCS2 with the ongoing transgression and onlap of the Jurassic deposits on the Arabian Platform. Paleoecological conditions are so complex that it is dangerous to use biodiversity as the main indicator for MFS hierarchy.

The top sequence boundary of the Marrat sequences corresponds to a regional hiatus over the Arabian Platform, in the late Toarcian–Aalenian, that relates to a substantial eustatic sea-level fall (Le Nindre et al., 1990; Al-Husseini, 1997; Jacquin et al., 1998; Simmons et al., 2007; Ogg and Hinnov, 2012; Haq and Al-Qahtani, 2005; Haq, 2018; Simmon and Davies, 2018) and/or subsidence resistance and large-scale uplift (Le Nindre et al., 2003; Al-Mojel et al., 2018) or relative sea-level stillstand with infill of accommodation space by the sediments. The lack of any incision during this long-term hiatus suggests that there is no major high amplitude sea-level fall during this period. This hiatus is widespread in the Tethyan domain which is possibly related to thermal basaltic doming in the North Sea with volcanic activities associated with subsequent collapse (Hallam, 2001). In detail, these two composite sequences MCS1 and MCS2 could correspond to the Tethyan eustatic sequences Toa3 and Toa4 of Hardenbol et al. (1998), which considered as 3rd-order cycle of ~1.6 Myr influenced by astronomical forcing controls,

precession and obliquity including their long-term modulations (Hinnov and Park, 1999; Boulila et al., 2014).

The short-term fluctuation of relative sea-level changes recorded on the Arabian Platform during deposition time of the Marrat Formation range from 15 to 25 m (calculated from relative sea-level amplitude of Haq and Al-Qahtani, 2005). This gives an average rate of 0.08 m/kyr, which correspond to a moderate amplitude of relative sea-level changes (>15 m; Read, 1995, 1998). Whereas the cause of such moderate sea-level changes in warm greenhouse periods is still debated. It is most likely related to aquifer-eustasy (Wendler et al., 2016; Sames et al., 2016). An alternative scenario for the origin of this moderate amplitude of relative sea-level is the onset opening and sea floor spreading of the Atlantic Ocean (Hallam, 2001).

7.2.3 Climatic influences

During the Early Jurassic, the Arabian Platform was situated along the tropical belt probably a few degrees south of the Equator (Fig. 2; Murris, 1980; Thierry et al., 2000; Sharland et al., 2001) Here, the study of the Toarcian sediments from the Marrat Formation allow us to address for the first time the impact of these climatic disturbances in a coastal/inner-platform context situated at very low paleolatitudes. Among the Jurassic climate changes (Dera et al., 2011), the early Toarcian warming event is generally considered as the warmest interval, as current numerical models suggest rapid temperature rises of +5 to +10°C in terrestrial domains (Dera and Donnadieu, 2012). This episode was also documented in marine paleoenvironments from European domains with shifts in the oxygen isotope composition of various fossils (Bailey et al., 2003, van de Schootbrugge et al., 2005; Suan et al.,

2010). Probably initiated by considerable CO_2 releases from Karoo-Ferrar volcanism and subsequent clathrate destabilization on the seafloor (Hesselbo et al., 2000), this disturbance is further believed to have caused a redistribution of humid belts toward mid- and high-latitudes (Dera et al., 2015), and global increases of weathering rates (Cohen et al., 2004, Dera et al., 2009). Occurrence of fluvial systems during the Lower Marrat transgression (MCS1) with plant fragments, high kaolinite (Abed, 1979) and high gamma-ray response (Fig. 13) suggest humid period which corresponded to the initial warm peak of the early *serpentinum* Zone (Fig. 15). The humid period evolved to more semi-arid condition during late TST and MFS of MCS1 evident by stromatolites, mudcracks with limited siliciclastic influx and later with carbonate development. The semi-arid condition and the carbonate development could be related to slight decrease of the paleotemperature during late *serpentinum* Zone (Fig. 15; Gomez and Goy, 2011). The regressive evolution recorded in the Middle Marrat (turn-over between MSC1 and MSC2) with the deposition of thick and extensive kaolinite and hematite enrichments of reddish shale (Abed, 1979) and sandstone deposits cannot be considered as a response to the decrease of accommodation rate but to an increase of the terrigenous influx. This shale-dominated influx could be interpreted as indicative of strong hydrolyzing conditions under humid and warm conditions (Chamley, 1989). These observations are thus compatible with numerical simulation suggesting rises in precipitation and runoff rates (+5 to 15 cm/kyr) on the southern part of the Arabian craton (Dera and Donnadieu, 2012). The Middle Marrat could be really the best record of an increase of humidity during the early Toarcian warm period (Fig. 15). In the

same way, the MCS2 transgression could be favored by a combination of eustatic transgression (*bifrons* Zone) and decrease of the siliciclastic input indicating more semi-arid conditions with possible simultaneous overall decrease in paleotemperature during the *bifrons* Zone (Fig. 15). Remarkably, the synchronicity of the TST and MFS with semi-arid and cooling events and HST with humid warm condition provides some confidence to the aquifer-eustasy as primary mechanism controlling these 3rd-order sea-level changes (cf. Wendler et al., 2016; Sames et al., 2016).

8 Conclusion

The outcrops of the Marrat Formation (early to middle Toarcian) in Saudi Arabia provide a stratigraphic record of the initial Jurassic transgression of a broad slowly subsiding epeiric tropical platform over the Triassic−Jurassic unconformity. The depositional environment ranges from continental meandering fluvial deposits to tidal or wave-dominated mixed carbonate-siliciclastic inner-platform deposits. These formed aggraded flat-topped platform wedging and thickening northward. Syndepositional differential subsidence has an influence on lateral thickness variation and facies distribution. The carbonates are mud-dominated facies and are preferentially formed in high subsidence areas with more accommodation space. The Marrat Formation is composed of two 3rd-order sequences and show progressive marine transgression that reach its maximum in the middle Toarcian *bifrons* Zone, consistent with the major MFS of the Early Jurassic of the Arabian Platform and the European major MFS. The layer-cake geometries are controlled by the low-energy wide platform with stable tectonic context, that leads for limited accommodation space filled by siliciclastic

supply and carbonate production. Short-lived higher energy siliciclastic shorelines and tidal-flat appear during high accommodation space in late-TST and HST. The carbonates are best developed during maximum marine transgression of the two Marrat sequences. High terrigenous influx event between these two sequences consists of aggraded extensive continental red shales and fluvial sandstone. This is possibly related to the strong hydrolyzing conditions under humid-warm period (early-middle Toarcian *bifrons* Zone rather than a decrease of accommodation space. The synchronicity of the regression with humid-warm periods provides some confidence to the aquifer-eustasy driver mechanism of the Marrat depositional sequences.

Acknowledgments

This work was part of a PhD thesis that was carried out at the University of Bordeaux-Montaigne, ENSEGID Bordeaux INP, and was sponsored by Saudi Aramco. We thank the management of Saudi Aramco for the permission to publish this work. We express our thankfulness and gratitude to Dr. Aus Al-Tawil (RCD manager, Saudi Aramco) for his endless outstanding support and motivations during all phases of this study. We also thank Dr. Denis Vaslet, Prof. J. Fred Read, Prof. Charles Kerans, Dr. Moujahed Al-Husseini and Dr. Langhorne Smith for providing valuable suggestions and constructive comments. Special thanks to Dr. Mohammed Al-Masrahy for significantly improving the article. We also extend our thanks to Dr. Mahmoud Al-Nazghah and Dr. Raed Al-Dukhayyil for field support.

References

Abdullah, F.H., Connan, J., 2002. Geochemical study of some Cretaceous rocks from Kuwait: comparison with oils from Cretaceous and Jurassic reservoirs. Organic geochemistry, 33(2), 125-148.

Abed, A.M., 1979. Lower Jurassic lateritic redbeds from central Arabia. Sedimentary Geology 24 (1), 149-156.

Al-Eidan, A., Neog, N., Narhari, S., Al-Darmi, A., Al-Mayyas, R., De Keyser, T., Perrin, C., 2009. Depositional Environments of the Marrat Formation (Lower Jurassic), North Kuwait. Search and Discovery Article, 50223, 7-10.

Al-Husseini, M.I., 1997. Jurassic sequence stratigraphy of the western and southern Arabian Gulf. GeoArabia (Manama), 2(4), 361–82.

Al-Husseini, M.I., 2000. Origin of the Arabian plate structures: Amar collision and Najd Rift. GeoArabia 5, 527–542.

Al-Husseini, M.I., 2009. Update to Late Triassic-Jurassic stratigraphy of Saudi Arabia for the Middle East geologic time scale. GeoArabia 14(2), 145-186.

Al-Husseini, M.I., Matthews, R.K. 2008. Jurassic-Cretaceous Arabian orbital stratigraphy: The AROSJK Chart, GeoArabia, 13 (1), 89-94.

Al-Masrahy M.A., Mountney N.P., 2015. Quantitative approach to the characterization of sedimentary architecture in mixed eolian-fluvial reservoir successions, Search and Discovery Article 41669. 1-4.

Al-Mojel, A., 2017. Sedimentology and sequence stratigraphy of the Jurassic, Jebal Tuwaiq, Central Saudi Arabia. Ph.D. Thesis, Univ. Bordeaux 3, Bordeaux, France.

Al-Mojel, A., Dera, G., Razin, P., Le Nindre, Y.M., 2018. Carbon and oxygen isotope stratigraphy of Jurassic platform carbonates from Saudi Arabia: Implications for diagenesis, correlations and global paleoenvironmental changes. Palaeogeography, Palaeoclimatology, Palaeoecology. In press.

Al-Sharhan, A.S., Strohmenger, C.J., Al-Mansoori, A.A., 2014. Mesozoic petroleum systems of Abu Dhabi, United Arab Emirates. In: Marlow, L., Kendall, C., Yose, L., (Eds.), Petroleum systems of the Tethyan region: AAGP Memoir 106, 679-711.

Allen, J.R.L., 1982. sedimentary structures: their character and physical basis, Volume 1. Elsevier, Amsterdam. 611.

Alsharhan, A.S., Nairn, A.E.M., 1994. The Late Permian carbonates (Khuff Formation) in the western Arabian Gulf: Its hydrocarbon parameters and paleogeographical aspects. Carbonates and Evaporites, 9(2), 132.

Alsharhan, A.S., Nairn, A.E.M., 2003. Sedimentary basins and petroleum geology of the Middle East. Elsevier, Amsterdam, 843 pp.

Aqrawi, A., Goff, J.C., Horbury, A., Sadooni, D., 2010. The petroleum Geology of Iraq. Beaconsfield, UK, Scientific Press, 424.

Ayres, M.G., Bilal, M., Jones, R.W., Slentz, L.W., Tartir, M., Wilson, A.O., 1982. Hydrocarbon habitat in main producing areas, Saudi Arabia. AAPG bulletin, 66(1), 1-9.

Bailey, T.R., Rosenthal, Y., McArthur, J.M., Van de Schootbrugge, B., Thirwall, M.F., 2003. Paleoceanographic changes of the Late Pliensbachian–Early Toarcian interval: a possible link to the genesis of an

940 Oceanic Anoxic Event. Earth and Planetary Science Letters, 212, 307–
941 320.
942 Banerjee, I. 1991. Tidal sand sheets of the Late Albian Joli Fou-Kiowa-Skull
943 Creek Marine transgression, Western Interior Seaway of North America.
944 335-347.
945 Banham, S.P., Mountney, N.P. 2014, Climatic versus halokinetic control on
946 sedimentation in a dry land fluvial succession. Sedimentology 61, 570-
947 608.
948 Baud, A., Droste, H., Guillocheau, F., Razin, P., Robin, C., 2005. Mesozoic
949 Evolution of the Tethyan margin of Oman. In 24th IAS regional Meeting,
950 Pre-Conference Excursion BF. 4.
951 Baudin, F., Herbin, J.P., Bassoullet, J.P., Dercourt, J., Lachkar, G., Manivit,
952 H., Renard, M., 1990. Distribution of organic matter during the Toarcian in
953 the Mediterranean Tethys and Middle East. In Deposition of organic
954 facies, The American Association of Petroleum Geologists, 30, 73-91.
955 Blum, M.D., Törnqvist, T.E., 2000. Fluvial responses to climate and sea-level
956 change: a review and look forward. Sedimentology, 47, 2-48.
957 Bott, M.H.P., 1992. Passive margins and their subsidence. Journal of the
958 Geological Society, 149(5), 805-812.
959 Bottjer, D.J., Arthur, M.A., Dean, W.E., Hattin, D.E., Savrda, C.E., 1986.
960 Rhythmic bedding produced in Cretaceous pelagic carbonate
961 environments; sensitive recorders of climatic cycles. Paleoceanography,
962 1(4), 467-481
963 Boulila, S., Galbrun, B., Huret, E., Hinnov, L. A., Rouget, I., Gardin, S.,
964 Bartolini, A., 2014. Astronomical calibration of the Toarcian Stage:
965 implications for sequence stratigraphy and duration of the early Toarcian
966 OAE. Earth and Planetary Science Letters, 386, 98-111.
967 Bramkamp, R.A., Steineke, M., 1952. Stratigraphical introduction. In: Arkell,
968 W.J., Bramkamp, R.A., Steineke, M. (Eds.), Jurassic Ammonites from
969 Jebel Tuwaiq, Central Arabia. Royal Society [London] Philosophical
970 Transactions B 236, 241–313.
971 Bridge, J.S., 2006. Fluvial facies models: recent developments. In: H.W.,
972 Walker, R.G., (Ed.), Facies models revisited. International Association of
973 Sedimentologists, Special Publication 84, 85-170.
974 Bromley, R.G., Ekdale, A.A., 1984. Trace fossil preservation in flint in the
975 European chalk. Journal of Paleontology, 58, 298–311.
976 Chamley, H., 1989. Clay Sedimentology. Springer Verlag, Berlin.
977 Church, M. 2006. Bed material transport and the morphology of alluvial river
978 channels. The Annual Review of Earth and Planetary Science, 34, 325–
979 354.
980 Clarke, M.W.H., 1988. Stratigraphy and rock unit nomenclature in the oil-
981 producing area of interior Oman. Journal of Petroleum Geology, 11(1), 5-
982 60.
983 Cohen, A.S., Coe, A.L., Harding, S.M., Schwark, L., 2004. Osmium isotope
984 evidence for the regulation of atmospheric CO2 by continental
985 weathering. Geology 32 (2), 157–160.
986 Collinson, J.D., 1996. Alluvial sediments. In: Reading, H.G. (Ed.),
987 Sedimentary Environments: Processes, Facies and Stratigraphy,
988 Blackwell Science, 37-82.

Crevello, P. D., 1990, Depositional systems tracts, stacking patterns, and sequence stratigraphy of Lower and Middle Jurassic synrift carbonate platforms, Central and Eastern High Atlas, Morocco. International Association of Sedimentologists, 1990 Annual Meeting, Proceedings with Abstracts, 111-112.

Davies, R.B., Casey, D.M., Horbury, A.D., Sharland, P.R., Simmons, M.D., 2002. Early to mid-Cretaceous mixed carbonate-clastic shelfal systems: Examples, issues, and models from the Arabian Plate. GeoArabia 7, 541-598.

Davis Jr, R.A., 2012. Tidal signatures and their preservation potential in stratigraphic sequences. In: Davis Jr. R.A., Dalrymple, R.W. (Eds.), Principles of tidal sedimentology. Springer, Netherlands, 35-55.

Delvaux, D., 2001. Karoo rifting in western Tanzania: Precursor of Gondwana breakup. Contributions to geology and paleontology of Gondwana in honor of Helmut Wopfner: Cologne, Geological Institute, University of Cologne, 111-125.

Dera, G., Brigaud, B., Monna, F., Laffond, R., Puceat, E., Deconinck, J.F., Pellenard, P., Joachimsky, M., Durlet, C., 2011. Climatic ups and downs in a disturbed Jurassic world. Geology 39, 215-218.

Dera, G., Donnadieu, Y., 2012. Modeling evidences for global warming, Arctic seawater freshening, and sluggish oceanic circulation during the Early Toarcian anoxic event. Paleoceanography, 27(2).

Dera, G., Pellenard, P., Neige, P., Deconinck, J. F., Pucéat, E., Dommergues, J. L. 2009. Distribution of clay minerals in Early Jurassic Peritethyan seas: palaeoclimatic significance inferred from multiproxy comparisons. Palaeogeography, Palaeoclimatology, Palaeoecology, 271(1), 39-51.

Dera, G., Prunier, J., Smith, P. L., Haggart, J. W., Popov, E., Guzhov, A., Rogov, M., Delsate, D., Thies, D., Cuny, G., Pucéat, E., Charbonnier, D., Bayon, G., 2015. Nd isotope constraints on ocean circulation, paleoclimate, and continental drainage during the Jurassic breakup of Pangea. Gondwana Research, 27(4), 1599-1615.

Dumas, S., Arnott, R.W.C., 2006. Origin of hummocky and swaley cross-stratification−The controlling influence of unidirectional current strength and aggradation rate. Geology, 34(12), 1073-1076.

Dunham, R.J., 1962. Classification of carbonate rocks according to depositional texture. In: Ham, W.E. (Ed.), Classification of Carbonate Rocks: AAPG Memoir 1, 108-121. Tulsa, OK.

Embry, A.F., 1995. Sequence boundaries and sequence hierarchies: problems and proposals. In: Steel, R.J., Felt, V.L., Johannessen, E.P., Mathieu, C. (Eds.), Sequence stratigraphy on the Northwest European Margin. Special Publication, vol. 5. Norwegian Petroleum Society, pp. 1–11.

Embry, A.F., Klovan, J.E., 1971. A late Devonian reef tract on northeastern Banks Island, NWT. Bulletin of Canadian Petroleum Geology, 19(4), 730-781.

Énay, R., Y.-M. Le Nindre, C. Mangold, J. Manivit and D. Vaslet 1986. The Jurassic of central Saudi Arabia: New data on lithostratigraphic units, palaeoenvironments, ammonite faunas, ages and correlations. Deputy

Ministry of Mineral Resources, Jiddah, Technical Record BRGM-TRO6-3, 65 p.
Énay, R., Y.M. Le Nindre, C. Mangold, J. Manivit and D. Vaslet 1987. Le Jurassique d'Arabie Saoudite centrale: nouvelles données sur la lithostratigraphie, les paléoenvironnements, les faunes d'ammonites, les âges et les corrélations. Geobios, Lyon, Special Memoir 9, p. 13-65.
Fischer, J.-C., Manivit, J., Vaslet, D., 2001. Jurassic gastropod faunas of central Saudi Arabia. GeoArabia (Manama), 6(1), 63–100.
Fisher, J.A., Krapf, C.B.E., Lang, S.C., Nichols, G.J. and Payenberg, T.H.D., 2008. Sedimentology and architecture of the Douglas Creek terminal splay, Lake Eyre, central Australia. Sedimentology 55, 1915-1930
Frey, R. W. (ed.). 1975. The study of trace fossils: a synthesis of principles, problems, and procedures in ichnology. New York, Springer-Verlag.
Friend, P.F., Slater, M.J., Williams, R.C., 1979. Vertical and lateral building of river sandstone bodies, Ebro Basin, Spain. Geological Society of London136, 39-46.
Galli, G., 1993. "Calcari Grigi" formation, Jurasic, Venetian Alps. In: Galli, G. (Ed.), Temporal and Spatial Patterns in Carbonate Platforms. Springer, Berlin, 97-129.
Gerard, J., Bromley, R., 2008. Ichnofabrics in clastic sediments: applications to sedimentological core studies (p. 100). Madrid: J. Gerard.
Gibling, M.R., 2006. Width and thickness of fluvial channel bodies and valley fills in the geological record: A literature compilation and classification. Journal of Sedimentary Research 76, 731-770.
Ginsburg, R. N., 1975. Tidal deposits: a casebook of recent examples and fossil counterparts. Springer Science & Business Media.
Glennie, K.W., Boeuf, M.G.A., Hughes-Clarke, M.W., Moody-Stuart, M., Pilaar W., Reinhardt, B.M., 1995. Late Cretaceous nappes in Oman Mountains and their geological evolution. AAPG Bulletin, 57, 5-27.
Gómez, J.J., Goy, A., 2011. Warming-driven mass extinction in the Early Toarcian (Early Jurassic) of northern and central Spain. Correlation with other time-equivalent European sections. Palaeogeography, Palaeoclimatology, Palaeoecology, 306(3), 176-195.
Gradstein, F.M., Ogg, J.G., Schmitz, M.D., Ogg, G.M., 2012. The Geologic Time Scale 2012. Elsevier, p. 1144.
Hallam, A., 2001. A review of the broad pattern of Jurassic sea-level changes and their possible causes in the light of current knowledge. Palaeogeography, Palaeoclimatology, Palaeoecology, 167(1), 23-37.
Haq, B.U., 2018. Jurassic sea-level variations: a reappraisal. GSA Today, 28(1).
Haq, B.U., Al-Qahtani, A.M., 2005. Phanerozoic cycles of sea-level change on the Arabian Platform. GeoArabia, 10(2), 127-160.
Haq, B.U., Hardenbol, J., Vail, P.R., 1987. Chronology of fluctuating sea levels since the Triassic. Science, 235 (4793), 1156-1167.
Haq, B.U., Hardenbol, J., Vail, P.R., 1988. Mesozoic and Cenozoic chronostratigraphy and cycles of sea-level change. SEPM Special Publications 42, 71–108.
Hardenbol, J., Jacquin, T., Farley, M.B., de Graciansky, P.C., Vail, P.R., 1998. Mesozoic and Cenozoic sequence chronostratigraphic framework of

European basins. In: de Graciansky, P. C., Hardenbol, J., Jaquin, T., Vail, P.R. (Eds.), Mesozoic and Cenozoic Sequence Stratigraphy of European Basins. Society for Sedimentary Geology (SEPM), Tulsa, 3–13.

Harms, J.C., Southard, J.B., Spearing, D. R., Walker, R. G., 1975, Depositional environments as interpreted from primary sedimentary structures and stratification sequences: SEPM Short Course No. 2, 161 p.

Hatano, N., Yoshida, K., 2017. Sedimentary environment and paleosols of middle Miocene fluvial and lacustrine sediments in central Japan: Implications for paleoclimate interpretations. Sedimentary geology, 347, 117-129.

Hesselbo, S.P., Gröcke, D.R., Jenkyns, H.C., Bjerrum, C.J., Farrimond, P., Morgans Bell, H.S., Green, O.R., 2000. Massive dissociation of gas hydrate during a Jurassic oceanic anoxic event. Nature 406, 392–395.

Hinnov, L. A., Park, J. J., 1999. Strategies for assessing Early-Middle (Pliensbachian-Aalenian) Jurassic cyclochronologies. Philosophical Transactions of the Royal Society of London A: Mathematical, Physical and Engineering Sciences, 357(1757), 1831-1859.

Horbury, A., 2018. Petroleum geology and its relation to stratigraphic architecture of the Triassic to Middle Jurassic (Induan to Aalenian) Interval on the Arabian Plate. In: Pöppelreiter, M.C. (Ed.), Lower Triassic to Middle Jurassic Sequence of the Arabian Plate. EAGE, 49-100.

Hunt, D., Tucker, M.E., 1993. Sequence stratigraphy of carbonate shelves with an example from the mid-Cretaceous (Urgonian) of southeast France. Sequence stratigraphy and facies associations, 307-341.

Issautier, B., Le Nindre, Y. M., Abdullah, M., Saleh, D., Sophie, V., 2012. Managing clastic reservoir heterogeneity I: sedimentology and sequence stratigraphy of the Minjur Sandstone at the Khashm-al-Khalta type locality (Central Saudi Arabia). GeoArabia, 17(2), 17-56.

Issautier, B., Le Nindre, Y., Memesh, A., Dini S., Viseur, S., 2012a. Managing clastic reservoir heterogeneity, I: Sedimentology and sequence stratigraphy of the Late Triassic Minjur Sandstone at the Khashm al Khalta type locality Central Saudi Arabia. GeoArabia 17(2), 17-56.

Issautier, B., Le Nindre, Y., Viseur S., Memesh, A., Dini, S., 2012b. Managing clastic reservoir heterogeneity, II: Geological modelling and reservoir characterization of the Minjur Sandstone at the Khashm Al Khalta type locality, Central Saudi Arabia. GeoArabia 17(3), 61-80.

Jacquin, T., Dardeau, G., Durlet, C., de Graciansky, P.C., Hantzpergue, P., 1998. The North Sea cycle: an overview of 2nd-order transgressive/regressive facies cycles in western Europe. In: de Graciansky, P-C., Hardenbol, J., Jacquin, T., Vail, P.R. (Eds.), Mesozoic an overview of 2nd order transgressive/regressive facies cycles in Western Europe. SEPM, Special Publication (60), 397-410.

Jenkyns, H.C., Sarti, M., Masetti, D., and Howarth, M.K., 1985, Ammonites and stratigraphy of Lower Jurassic black shales and pelagic limestones from the Belluno trough, southern Alps: Ecologae Geologicae Helvetiae, 78, 299-311.

Kadar, A.P., De Keyser, T., Neog, N., Karam, K.A., Le Nindre Y.M., Davies, R.B., 2015. Calcareous nannofossil zonation and sequence stratigraphy of the Jurassic System, onshore Kuwait. GeoArabia, 20(4), 125-180.

Kerans, C., Tinker, S.W., 1997. Sequence stratigraphy and characterization of carbonate reservoirs. Society of Sedimentary Geology: SEPM Short Course Notes, 40.

Khalifa, M.A., 2007. Triassic-Jurassic boundary on the southern margin of Tethys: implications of facies, tectonics and volcanism. In: Lucas, S.G., Spielmann, J.A. (Eds.), The Global Triassic. New Mexico Museum of Natural History and Science, Bulletin 41, 110-119.

Khetani, A.B., Read, J.F., 2002. Sequence development of a mixed carbonate-siliciclastic high-relief ramp, Mississippian, Kentucky, USA. Journal of Sedimentary Research, 72(5), 657-672.

Kraus, M. J., 1999. Paleosols in clastic sedimentary rocks: their geologic applications. Earth-Science Reviews, 47(1-2), 41-70.

Le Métour, J., Rabu, D., Tegyey, M., Béchennec, F., Beurrier, M., Villey, M., 1990. Subduction and obduction: two stages in the Eo-Alpine tectonometamorphic evolution of the Oman Mountains: In Robertson, A.H.F, Searle, M. P., Ries, A.C. (Eds), The Geology and Tectonics of the Oman Region: Geological Society of London, Special Publication 49, 327-340.

Le Nindre, Y.M., Manivit, J., Manivit, H., Vaslet, D., 1990. Stratigraphie sequentielle du Jurassique et du Cretace en Arabie Saoudite. Bulletin Société Géologique France, Paris 6, 1025-1035.

Le Nindre, Y.M., Vaslet, D., Le Métour, J., Bertrand, J., Halawani, M., 2003. Subsidence modelling of the Arabian Platform from Permian to Paleogene outcrops. Sedimentary Geology, 156, 263-285.

Leckie, D.A., Walker, R.G., 1982. Storm-and tide-dominated shorelines in Cretaceous Moosebar-Lower Gates interval--outcrop equivalents of Deep Basin gas trap in western Canada. AAPG Bulletin, 66(2), 138-157.

Leckie, D.A., Walker, R.G., 1982. Storm-and tide-dominated shorelines in Cretaceous Moosebar-Lower Gates interval--outcrop equivalents of Deep Basin gas trap in western Canada. AAPG Bulletin, 66(2), 138-157.

Lukasik, J.J., James, N.P., McGowran, B., Bone, Y., 2000. An epeiric ramp: low-energy, cool-water carbonate facies in a Tertiary inland sea, Murray Basin, South Australia. Sedimentology, 47(4), 851-881.

Manivit J, Le Nindre Y.M., Vaslet D. (1990) Le Jurassique d'Arabie Centrale. In Histoire Gologique de la Bordure Occidentale de la Plate-forme Arabe. Volume 4. Document du BRGM n°194.

Manivit, J., Pellaton, C., Vaslet, D., Le Nindre, Y.M., Brosse, J.M., Fourniguet, J., 1985a. Geologic map of the Wadi al Mulayh quadrangle, sheet 22H, Kingdom of Saudi Arabia. Saudi Arabian Deputy Ministry for Mineral Resources Geosciences Map, GM-92, scale, 1(250,000), 1-32.

Manivit, J., Pellaton, C., Vaslet, D., Le Nindre, Y.M., Brosse, J.M., Breton, J.P., Fourniguet, J., 1985b. Geologic map of the Darma quadrangle, sheet 24H, Kingdom of Saudi Arabia. Saudi Arabian Deputy Ministry for Mineral Resources Geosciences Map, GM-101, scale, 1(250,000), 133.

McIlroy, D., 2004. Ichnofabrics and sedimentary facies of a tide-dominated delta: Jurassic Ile Formation of Kristin Field, Haltenbanken, offshore Mid-Norway. Geological Society, London, Special Publications, 228(1), 237-272.

McKee, E. D., 1966. Significance of climbing-ripple structure. US Geol. Surv. Prof. Papper, 550, 94-103.

McKee, E.D., 1966. Structures of dunes at White Sands National Monument, New Mexico (and a comparison with structures of dunes from other selected areas). Sedimentology 7, 1-69.
Miall, A. D., 1996, The geology of fluvial deposits: sedimentary facies, basin analysis and petroleum geology: Springer-Verlag Inc., Heidelberg, 582p.
Miall, A.D., 1977. A review of the braided river depositional environment. Earth Science Reviews 13, 1-32.
Miall, A.D., 1978. Fluvial sedimentology. Canadian Society Petroleum Geologists, Memoir 5,105-127.
Miller, W., 2007. Complex trace fossils. In Trace Fossils (pp. 458-465).
Murris, R.J., 1980. Middle East: Stratigraphic evolution and oil habitat. AAPG Bulletin, 64,597–618.
Ogg, J.G., Hinnov, L.A., 2012. Jurassic. In: Gradstein, F.M., Ogg, J.G., Schmitz, M., Ogg, G. (Eds.), The Geologic Time Scale 2012, 1st Edition (1), 731-791.
Olsen, H., Due, P.H., Clemmensen, L.B., 1989. Morphology and genesis of asymmetric adhesion warts- a new adhesion surface structure: Sedimentary Geology 61, 277-285.
Osman, M., Abdullatif, O., Bashri, M., Babikr, J., 2018. Geological outcrop modelling of the Minjur and Marrat Formations – Integration of sedimentology and LiDAR data, Central Saudi Arabia. In: Pöppelreiter, M.C. (Ed.), Lower Triassic to Middle Jurassic Sequence of the Arabian Plate. EAGE, 229-248.
Pöppelreiter, M., Sharp, R., Turner, M., Haggas, S., Lewis, S., 2018. Overview of the global geological setting and the exploration and development history of the lower Triassic to Middle Jurassic. In: Pöppelreiter, M.C. (Ed.), Lower Triassic to Middle Jurassic Sequence of the Arabian Plate. EAGE, 33-48.
Powers, R.W., 1968. Lexique Stratigraphique International, v.III, Asie, 10bl, Saudi Arabia. Centre National de la Recherche Scientifique, Paris, 177p.
Powers, R.W., Ramirez, L.F., Redmond, C.D., Elberg, E.L., 1966. Geology of the Arabian Peninsula, Geological Survey Professional Paper, 560-D, 147p.
Rabalais, N.N., Turner, R.E., Wiseman, W.J., & Boesch, D.F., 1991. A brief summary of hypoxia on the northern Gulf of Mexico continental shelf: 1985–1988. Geological Society, London, Special Publications, 58(1), 35-47.
Read, J.F. 1995. Overview of carbonate platform sequences, cycle stratigraphy and reservoirs in greenhouse and icehouse worlds. In: Read, J.F., Kerans, C., Weber, L.J., Sarg, J.F., and Wright F.W. (Eds.), Milankovitch sea level changes, cycles and reservoirs on carbonate platforms in greenhouse and icehouse worlds, SEPM Short Course Notes No. 35, 1-102.
Read, J.F., 1989. Controls on evolution of Cambrian-Ordovician passive margin, US Appalachians. In: Crevello, P.D., Wilson, J.L., Sarg, J.F., Read, J.F. (Eds.), Controls on Carbonate Platform and Basin Development, SEPM Special Publication, 44, 146–165.
Read, J.F., 1998. Phanerozoic carbonate ramps from greenhouse, transitional and ice-house worlds: clues from field and modelling studies. Geological Society, London, Special Publications, 149(1), 107-135.

Reineck, H.E., Singh, I.B., 1980. Depositional Sedimentary Environments. Springer-Verlag, Berlin, Heidelberg, New York, p. 549.
Rubin, D.M., 1987. Cross-bedding, bedforms and palaeocurrents. Society of Economic Paleontologists and Mineralogists Concepts in Sedimentology and Paleontology 1, 187.
Sames, B., Wagreich, M., Wendler, J.E., Haq, B.U., Conrad, C.P., Melinte-Dobrinescu, M.C., Hu, X., Wendler, I., Wolfgring, E., Yilmaz, I.Ö., Zorina, S.O. 2016. Review: short-term sea-level changes in a greenhouse world−a view from the Cretaceous. Palaeogeography, Palaeoclimatology, Palaeoecology, 441, 393-411.
Sarg, J.F., 1988. Carbonate sequence stratigraphy. In sea level changes: an integrated approach. Society of Economic Paleontologists and Mineralogists Special Publication, 42, 155–181.
Sharland, P.R., Archer R., Casey D.M., Davies R.B., Hall S.H., Heward A.P., Horbury A.D., Simmons M.D., 2001. Arabian Plate Sequence Stratigraphy. GeoArabia Special Publication 2, Gulf PetroLink, Bahrain, 371.
Simmon, M.D., Sharland, P.R., Casey, D.M., Davies, R.B., Sutcliffe, O.E., 2007. Arabian Plate sequence stratigraphy: potential implications for global chronostratigraphy. GeoARabia (12), 101-130.
Simmons, M.D., Davies, R.B., 2018. Triassic to Middle Jurassic stratigraphy of the Arabian plate: an introduction. In: Pöppelreiter, M.C. (Ed.), Lower Triassic to Middle Jurassic Sequence of the Arabian Plate. EAGE, 1-32.
Soltan, R., Mountney, N.P., 2016. Interpreting complex fluvial channel and barform architecture: Carboniferous Central Pennine Province, northern England. Sedimentology, 63(1), 207-252.
Stear W. M., 1985. Comparison of the bedform distribution and dynamics of modern and ancient sandy ephemeral flood deposits in the southwestern Karoo Region, South Africa. Sedimentary Geology 45, 209-230
Stewart, S.A., Reid, C.T., Hooker, N.P., Kharouf, O.W., 2016. Mesozoic siliciclastic reservoirs and petroleum system in the Rub'Al-Khali basin, Saudi Arabia. AAPG Bulletin, 100(5), 819-841.
Suan, G., Mattioli, E., Pittet, B., Lécuyer, C., Suchéras-Marx, B., Duarte, L.V., Philippe, M., Reggiani, L., Martineau, F., 2010. Secular environmental precursors to Early Toarcian (Jurassic) extreme climate changes. Earth and Planetary Science Letters, 290(3), 448-458.
Summerfield, M.A., 1985. Plate tectonics and landscape development on the African continent. In: Morisawa, M., Hack, J. (Eds.), Tectonic Geomorphology. Allen and Unwin, Boston, 27-51.
Tang, D.Z., Lawrence, P., Gregory, A.E., Bakhiet, A.F.M., Bhullar, A.G., Ahmed, A., Macurda, B., 2010. Stratigraphic Framework and Exploration Potential of Early Jurassic Marrat Formation, Northern Saudi Arabia (Abstract). Proceeding of the AAPG GEO Middle East Conference & Exhibition, Manama, Bahrain, March 7-10, 2010. AAPG Search and Discovery Article #90105.
Tankard, A. J., Hobday, D.K., 1977. Tide-dominated back-barrier sedimentation, early Ordovician Cape Basin, Cape Peninsula, South Africa. Sedimentary Geology, 18(1-3), 135-159.
Thierry, J., Barrier, E., Abbate, E., Ait-Ouali, R., Ait-Salem, H., Bouaziz, S., Canerot, J., Elmi, S., Geluk, M., Georgiev, G., Guiraud, R., Hirsch, F.,

Ivanik, M., Le Metour, J., Le Nindre, Y.M., Medina, F., Nikishin, A.M., Page, K., Panov, D.L., Pique, A., Poisson, A., Sandulescu, M., Sapunov, I.G., Seghedi, A., Soussi, M., Tarkowski, R.A., Tchoumatchenko, P.V., Vaslet, D., Volozh, Y.A., Voznezenski, A.,Walley, C.D., Ziegler,M., Ait-Brahim, L., Bergerat, F., Bracene, R., Brunet, M.F., Cadet, J.P., Guezou, J.C., Jabaloy, A., Lepvrier, C., Rimmele, G., Belaid, A., Bonneau, M., Boutakiout, M., Chellai, E., Coutelle, A., Fedan, B., Fekirine, B., Guillocheau, F., Julien, M., Kokel, F., Laadila, M., Lott, G.N., Lamarche, J., Mami, L., Mansy, J.L., Mascle, G., Meister, C., Mouty, M., Pascal, C., Robin, C., Sebrier, M., Sihamdi, N., Souhel, A., Stephenson, R., Vera, J.A., Vuks, V.J., Vrielynck, B., Olivet, J.L., 2000a. Map 8, Middle Toarcian (180–178Ma). In: Dercourt, J., et al. (Ed.), Atlas Peri-Tethys, Paleogeographical Maps. Paris.

Thomas, R.G., Smith, D.G., Wood, J.M., Visser, J., Calverley-Range, E.A., Koster, E.H., 1987. Inclined heterolithic stratification−terminology, description, interpretation and significance. Sedimentary Geology, 53 (1-2), 123-179.

Tintant, H., 1984. Autochtonie ou allochtonie chez les Céphalopodes. Mém. Géol. Univ. Dijon, 7 (1982): 257-271.

Vail, P.R., Audemard, F., Bowman, S.A., Eisner, P.N., Perez- Cruz, C., 1991. The stratigraphic signatures of tectonics, eustasy and sedimentology − an overview. In: Einsele, G., Ricken, W., Seilacher, A. (Eds.), Cycles and Events in Stratigraphy. Springer, Berlin, 617–659.

Van de Schootbrugge, B., McArthur, J.M., Bailey, T.R., Rosenthal, Y., Wright, J.D., Miller, K.G., 2005. Toarcian anoxic event: an assessment of global causes using belemnite C isotope records. Paleoceanography, 20(3), PA3008.

Vaslet, D., 1987, Geologic du Paleozoique; Permien Superieur, Trias, Jurassique; lithostratigraphic: in Histoire geologique de la bordure occidentale de la plate-fornie arabe du PaleozoIque inferieur au Jurassique superieur (Y.M. Le Nindre, J. Manivit and D. Vaslet, authors), DSc Thesis, University of Paris VI, 1, 413 p.

Vaslet, D., Brush, J.M., Breton, J.P., Manivit, J., Le Strat, P., Fourniguet, J., Shorbaji, H., 1988. Geologic map of the quadrangle Shaqra, sheet 25H .Kingdom of Saudi Arabia: Deputy Ministry for Mineral Resources Geoscience Map GM-120C , 29.

Vaslet, D., Delfour, J., Manivit, J., Le Nindre, Y.M., Brosse, J.M., Fourniguet, J., 1983. Geologic map of the Wadi Ar Rayn quadrangle, sheet 23 H, Kingdom of Saudi Arabia. Saudi Arabian Deputy Ministry for Mineral Resources, Jeddah, Geosciences Map, GM-63A.

Weimer, R.J., Howard, J.D., Lindsay, D.R., 1982. Tidal flats and associated tidal channels. Sandstone Depositional Environments: American Association of Petroleum Geologists, Memoir, 31, 191-245.

Wendler, J.E., Wendler, I., Vogt, C., Kuss, J., 2016. Link between cyclic eustatic sea-level change and continental weathering: Evidence for aquifer-eustasy in the Cretaceous. Palaeogeography, Palaeoclimatology, Palaeoecology, 441, 430-437.

Williams, H.D., Burgess, P.M., Wright, V.P., Della Porta, G., Granjeon, D., 2011. Investigating carbonate platform types: multiple controls and a continuum of geometries. Journal of Sedimentary Research, 81(1), 18-37.

Willis B.J., Behrensmeyer A.K., 1994. Architecture of Miocene overbank deposits in northern Pakistan. Journal of Sedimentary Research, 64. 60-67.
Wilson, J.L., 1975. Carbonate Facies in Geologic History. Springer-Verlag, New York, 471 pp.
Wilson, J.L., Jordan, C., 1983. Middle Shelf Environment. In: Scholle, P.A., Bebout, D.G., Moore, C.H. (Eds.), Carbonate Depositional Environments. American Association Petroleum Geologists Memoir, 33, 345–440.
Wright, V.P., 1986. Paleosols their recognition and interpretation. Oxford, Balkwell Scientific, 315.
Yousif, S., Nouman, G., 1997. Jurassic geology of Kuwait. GeoArabia, 2(1), 91-110.
Ziegler, M.A., 2001. Late Permian to Holocene Paleofacies evolution of the Arabian plate and its hydrocarbon occurrences. GeoArabia, 6, 445-504.

Figure captions

Figure 1: Geological map of the study area showing the Jurassic outcrops modified from Fischer et al. (2001), measured sections, faults and magnetic lineaments. The measured sections are: (1) Khashm Ad Dhibi (N 24.23492°, E 46.09877°), (2) Wadi Al Jufayr (N 23.89844°, E 46.17702°), (3) Faridat Balum (N 23.7114°, E 46.23652°), (4) Khashm Al Khalta (N 23.58547°, E 46.17834°), (5) Khashm Disman (N 23.42942°, E 46.22265°), (6) Wadi Birk (N23.13083°, E 46.35743°), (7) Fara'id al Ahmar (N 22.56072°, E 46.10331°), (8) Khashm Munayyifiyah (N 22.18176°, E 45.88079°), (9) Khashm Abu Al Jiwar (N 21.84332°, E 45.73633°). The faults are mapped in the 1:250,00-scale quadrangles of Wadi al Mulayh (Manivit et al., 1985a), Wadi Ar Rayn (Vaslet et al., 1983), Darma (Manivit et al., 1985b) and Shaqra (Vaslet et al., 1988). The name of the faults are: f1 Wadi Al Atk Lineament, f2 Al 'Amar Fault, f3 and f4 are belong to the Najd Fault System (Al- Husseini, 2000).

Figure 2: Toarcian paleogeographic map showing the area of study: Toarcian paleogeographic map showing the area of study located in the southern located in the southern margin of the Neo-Tethys Ocean (modified

from margin of the Neo-Tethys Ocean (modied from Thierry et al., 2000; Dera et al., 2009).

Figure 3: Lithostratigraphic, biostratigraphic and sequence stratigraphy of the Early Jurassic in Jabal Tuwaiq, Saudi Arabia. The biostratigraphical data is mainly ammonites, and includes: 1) *Protogrammoceras* sp*., Bouleiceras* sp.; 2) *Nejdia* sp. and *Hildoceras* sp., 3) *Euhoploceras* sp. and *Hyperlioceras* sp.; 4) *Shirbuirnia* sp*., Dorsetensia* sp*.* and *Sonninidae* sp*.* (Modified from Fischer et al., 2001).

Figure 4: Fluvial facies association in the Marrat Formation. A) Pebbly sandstone and conglomerates (F1), base of braided fluvial channel, base of the Marrat Formation, Wadi Al-Jufair, B and C) Medium to coarse grain trough cross bedded sandstone (braided channel).

Figure 5: Fluvial facies association in the Middle Marrat Formation. A) Stacked meandering channel-fills, scour base (s arrow), inclined heterolithic stratification (IHS) (sandstone/shale), Khashm Al Khalta, B) Close-up of the scour base (s arrow in figure A) shows the IHS, C) Abandoned channel-fill shows IHS of point bar marked by the lateral grain-size fining trends to the left, Khashm Disman, D) Siltstone and thin fine-grained sandstone beds (pen for scale), overbank, Faridat Balum, E) Close-up of the very small ripples shows climbing- ripple lamination, overbank, Faridat Balum, F) Thinly laminated red shale with silt laminae, flood plain/lake, Wadi Al Jufayr, G) Mottled red shale with root traces, paleosol, Khashm Munayyifiyah (Jacob's staff is 120 cm).

Figure 6: Coastal plain facies association (A-E), high-energy nearshore facies association (F-G). A) Mottled bluish green shale (mud flat/coastal

plain), Lower Marrat, Khashm Disman, B) Stromatolitic lime-mudstone marked at the top by mudcracks (d arrow), mud flat/coastal plain, Lower Marrat, Khashm Ad Dhibi, C) Bioturbated heterolithic silty sandstone shows nodular structure, mixed flat/coastal plain, Upper Marrat, Khashm Al Khalta, D) Small ripples with mud drapes, sand tidal-flat, Upper Marrat, Khashm Al Khalta (note pen for scale), E) Channel-fill sandstone with mud drapes (? IHS) from the same horizon of photo D, tidal creeks, F) Sandstone with *Skolithos* burrows (s arrows), sand tidal-flat/bars, Upper Marrat, Khashm Abu Al Jiwar, G) Sharp base massive sandstone with swaley cross-stratification, storm influenced shoreface, Upper Marrat, Faridat Balum, H) Close-up photo of the swaley cross-stratification in photo G shows chevron structure developed a ripple crest (arrow).

Figure 7: Mixed carbonate-siliciclastic inner-lagoon facies association in Khashm Ad Dhibi. A) Grayish green calcareous shale (shale dominated inner lagoon), Upper Marrat (note hammer for scale), B) Argillaceous nodular bioturbated peloidal wackestone/mudstone (carbonate dominated inner lagoon), Upper Marrat, C) Nodular horizontal-bioturbated peloidal wackestone (where the notebook is located) intercalated with highly bioturbated wackestone/mudstone beds, Middle Marrat, D) Top and side view of the bioturbated wackestone/mudstone (highly bioturbated lagoon), Middle Marrat.

Figure 8: Vertical facies successions show the evolution of the depositional environments (from fluvial to carbonate inner lagoon) during a 3rd-order marine transgression. A) The Lower Marrat outcrop photo from Wadi Al Jufayr, Marrat composite sequence 1 (MCS1), B) The Middle and Upper Marrat outcrop at Khashm Ad Dhibi, Marrat composite sequence 2 (MCS2).

Figure 9: Detailed measured section of the Marrat Formation, A) the lower and middle Marrat, Marrat composite sequence 1 (MCS1), at Wadi Al Jufayr section shows the onset of the Jurassic transgression over the Triassic−Jurassic unconformity. The MFS of MCS1 is placed in the highly bioturbated nodular peloidal wackestone/mudstone with Early Toarcian ammonite fauna, B) Fara'id al Ahmar measured section shows the two Marrat composite sequences MCS1 and MCS2, C) Khashm Munayyifiyah measured section shows the two Marrat composite sequences MCS1 and MCS2. Base MCS2 shows typical meandering vertical successions with fining-up trend. For symbol and facies color legend see Fig. 10, 11 and 12.

Figure 10: Detailed core description of the upper Marrat Formation at Khashm Ad Dhibi section (from DHIBI-1 outcrop core) combined with biofacies summary and paleoenvironmental interpretation (Hughes, 2009; unpublished Saudi Aramco report). The succession is characterized by mixed carbonate- siliciclastic cycles. This core is bounded at the base by fluvial deposits and at the top by a major unconformity. The section shows initial transgression over fluvial deposits. The upward-increasing proportion of the bioturbated carbonate lithofacies reflects an overall marine transgression trend. The MFS is placed in the thickest beds of highly bioturbated lime-mudstone.

Figure 11: Idealized block diagram shows the Marrat Formation facies distribution in relation to the shoreline position. The facies are deposited in very-wide flat inner-platform depositional environments. The diagram is not meant to show synchronous facies. This is because the depositional environments are evolving through the successions. For example, tidal creeks

and wide coastal plain were developed lately in the upper Marrat Formation. High-energy wave-dominated shoreline appears only during late TST, whereas early TST and HST are characterized by low-energy mud-dominated shoreline. The bathymetry was estimated by reconstructing the depositional profile from one of the upper cycles in the cross-section.

Figure 12: High-resolution sequence-stratigraphic cross section of the Marrat Formation along the Jabal Tuwaiq outcrops. The datum is top of the Marrat unconformity which is overlain by evaporite deposits in the northern area and silty ferruginous oolite deposits in the southern area. The latitudinal coordinates are shown at the head of the section as reference points. For ammonite names see (Fig. 8).

Figure 13: A) Sequence-stratigraphic correlation from surface to subsurface using gamma-ray logs. Detailed facies analysis and sequence stratigraphy of the Khashm Ad Dhibi are presented in (Figs. 3, 10 and 12) Paleofacies map of the Early Jurassic (Sinemurian to Aalenian) shows two correlation trajectories and approximate location of the Jurassic shelf margin (modified after Ziegler, (2001).

Figure 14: Toarcian geological history shows sequence stratigraphy of the Central Arabia compared with the European domain.

Figure 15: Comparison of facies and sequence stratigraphy of the studied area with average seawater paleotemperature of the European Epicontinental Sea. The average seawater paleotemperature calculated from several localities included in the European Epicontinental Sea (Gomez and Goy, 2011). Note: the Khashm Ad Dhibi section is rescaled to fit the paleotemperature curve.

1469

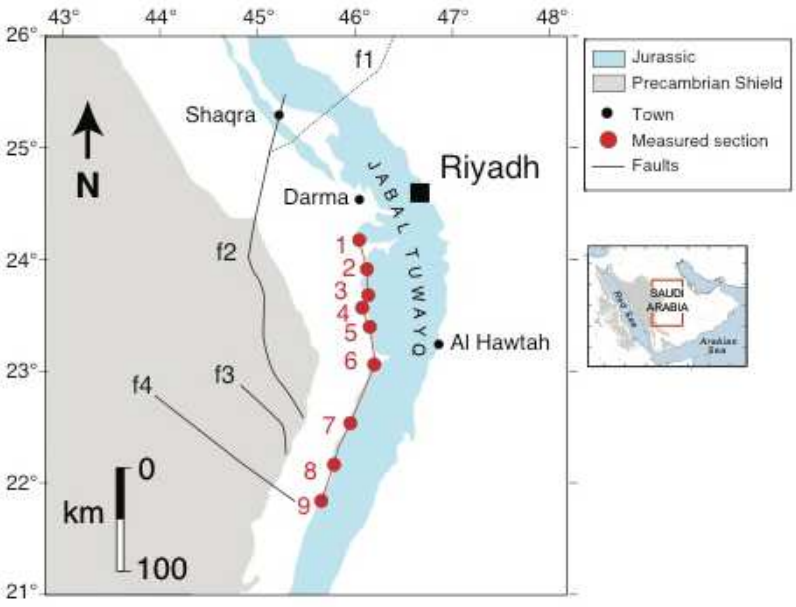

Figure 1

1470

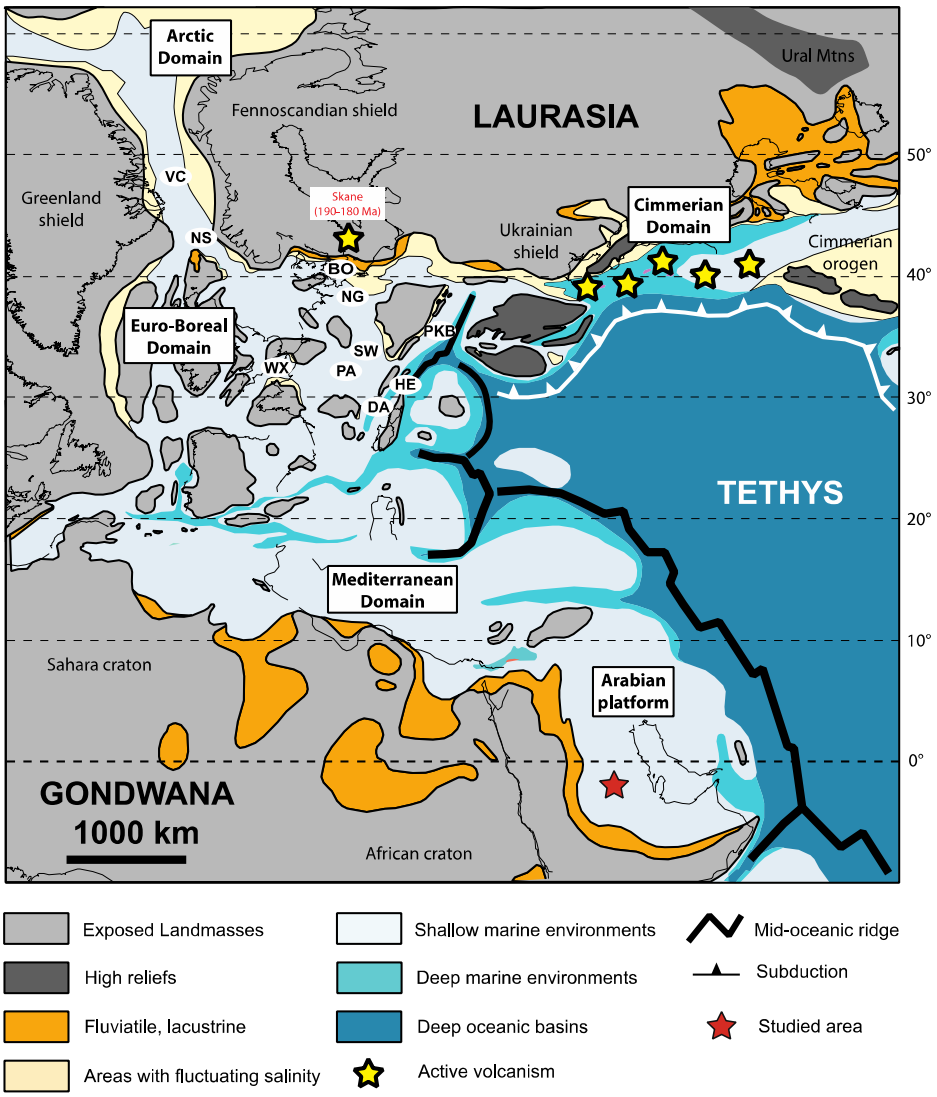

Figure 2

1471

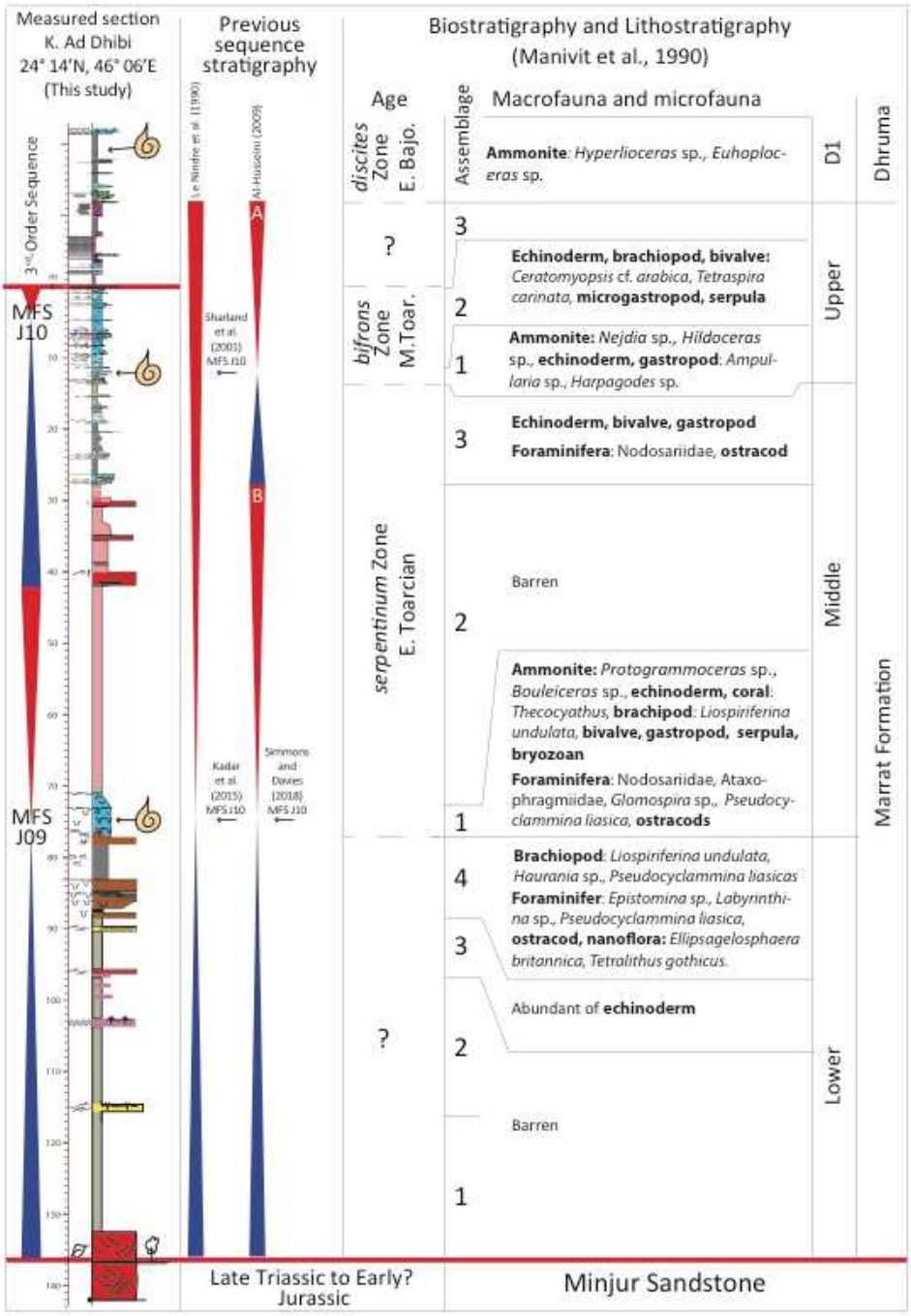
Measured section
K. Ad Dhibi
24° 14'N, 46° 06'E
(This study)
3rd Order Sequence
MFS J10
MFS J09
Previous sequence stratigraphy
Le Nindre et al. (1990)
Al-Husseini (2009)
A
B
Sharland et al. (2001) MFS J10
Kadar et al. (2015) MFS J10
Simmons and Davies (2018) MFS J10
Biostratigraphy and Lithostratigraphy
(Manivit et al., 1990)
Age
Assemblage
Macrofauna and microfauna
discites Zone E. Bajo.
bifrons Zone M.Toar.
serpentinum Zone E. Toarcian
?
3
2
1
3
2
1
4
3
?
2
1
Ammonite: Hyperlioceras sp., Euhoploceras sp.
Echinoderm, brachiopod, bivalve: Ceratomyopsis cf. arabica, Tetraspira carinata, microgastropod, serpula
Ammonite: Nejdia sp., Hildoceras sp., echinoderm, gastropod: Ampullaria sp., Harpagodes sp.
Echinoderm, bivalve, gastropod
Foraminifera: Nodosariidae, ostracod
Barren
Ammonite: Protogrammoceras sp., Bouleiceras sp., echinoderm, coral: Thecocyathus, brachipod: Liospiriferina undulata, bivalve, gastropod, serpula, bryozoan
Foraminifera: Nodosariidae, Ataxophragmiidae, Glomospira sp., Pseudocyclammina liasica, ostracods
Brachiopod: Liospiriferina undulata, Haurania sp., Pseudocyclammina liasicas
Foraminifer: Epistomina sp., Labyrinthina sp., Pseudocyclammina liasica, ostracod, nanoflora: Ellipsagelosphaera britannica, Tetralithus gothicus.
Abundant of echinoderm
Barren
D1
Upper
Middle
Lower
Dhruma
Marrat Formation
Late Triassic to Early? Jurassic
Minjur Sandstone

1472

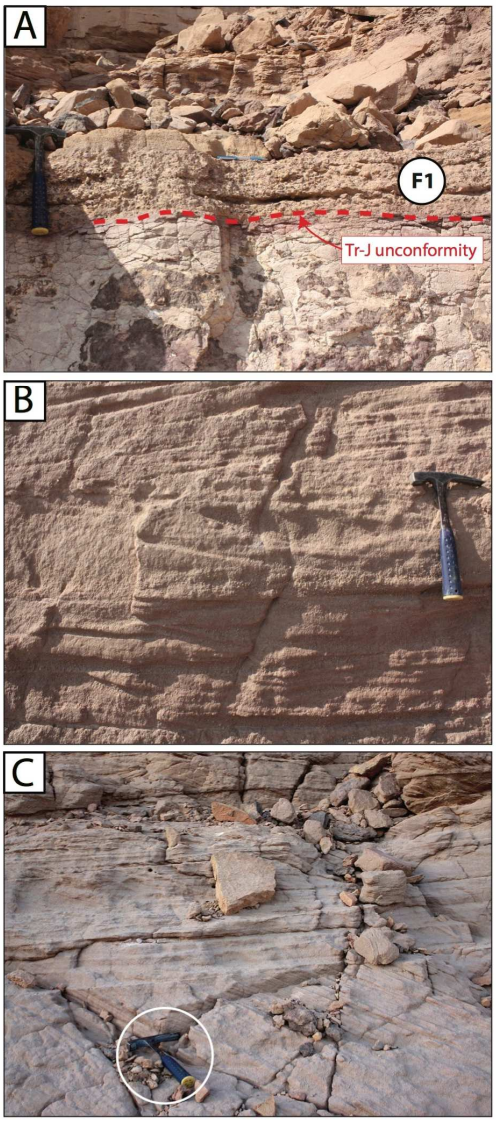

Figure 4

1473

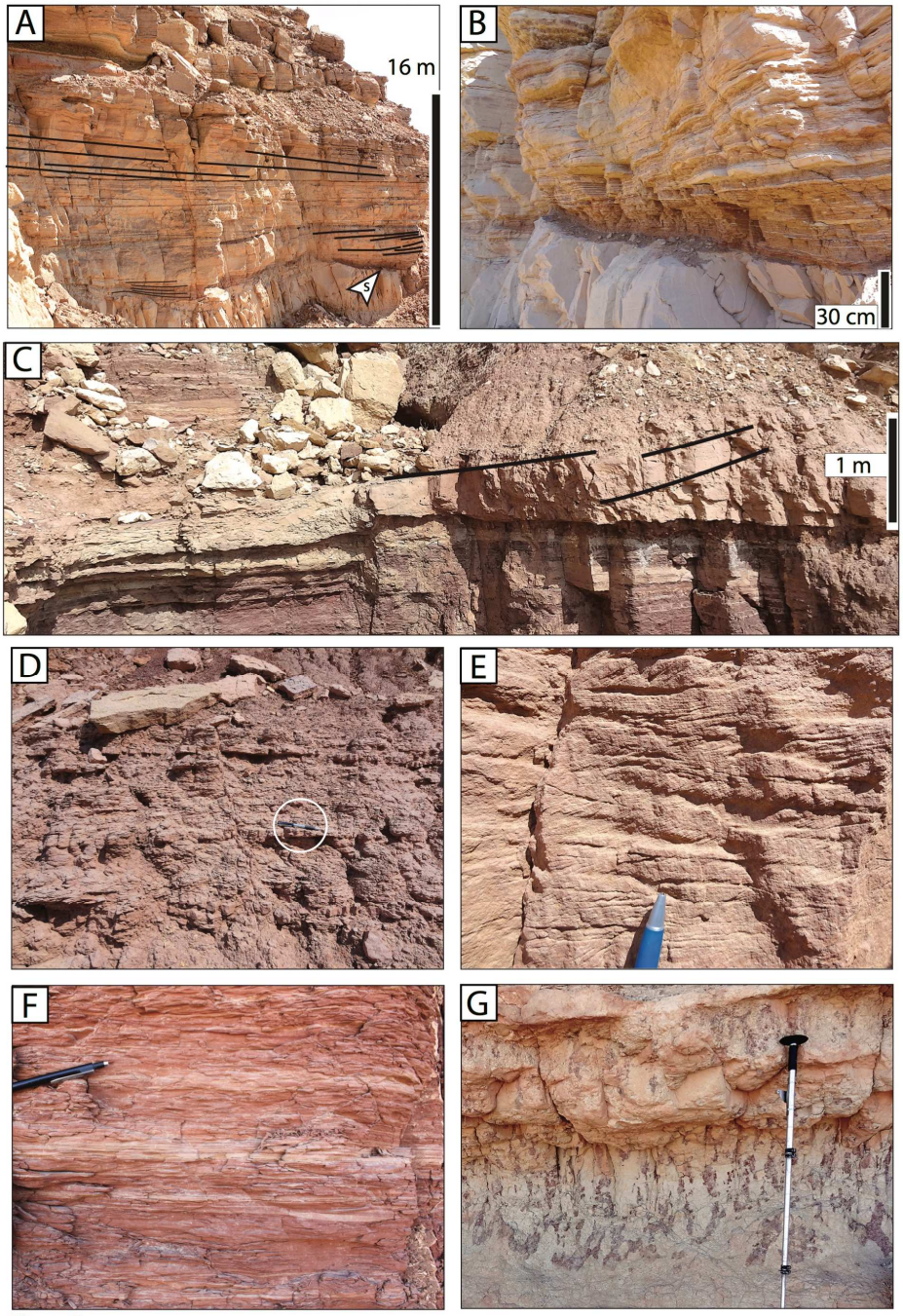

Figure 5

1474

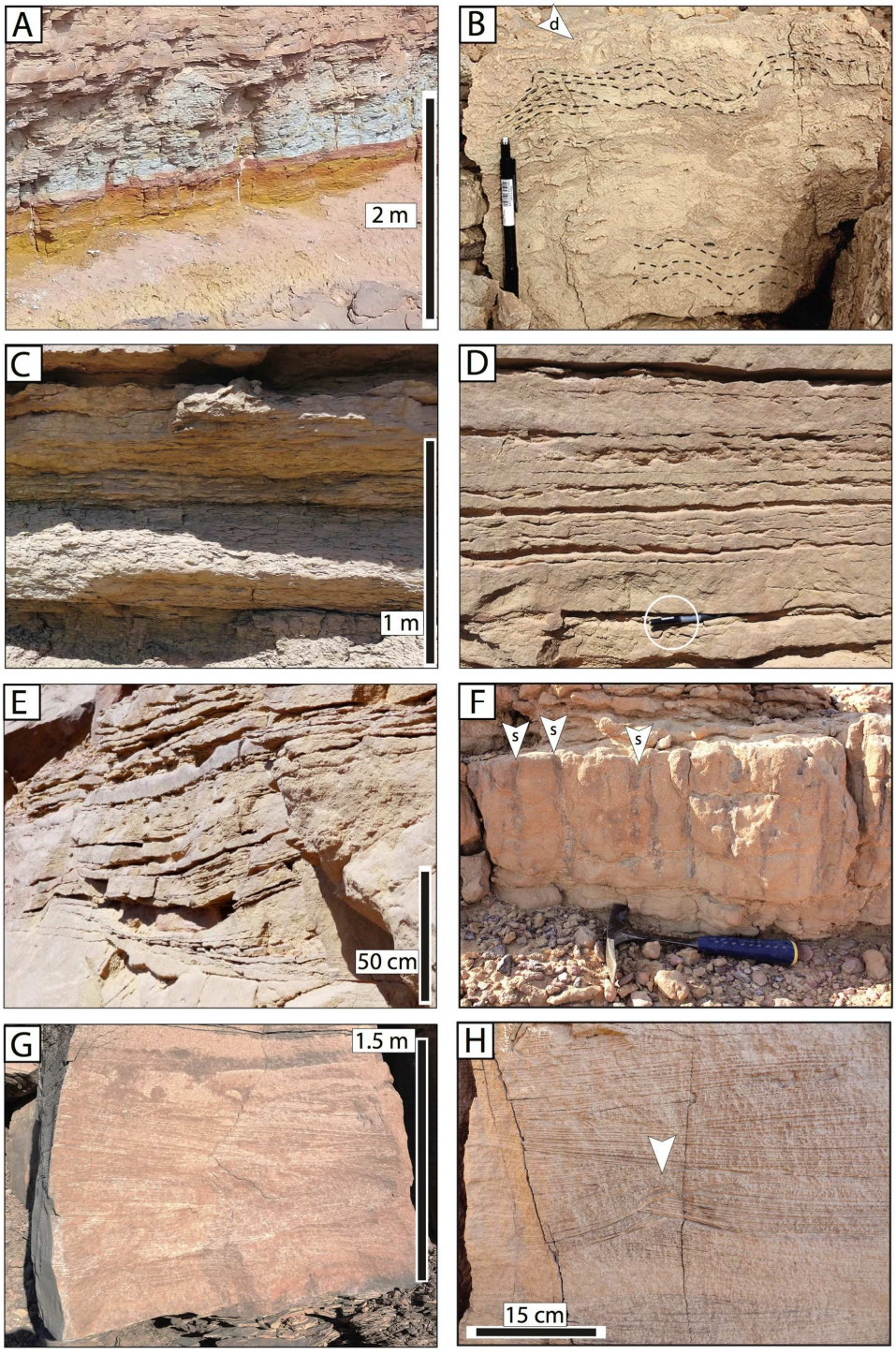

Figure 6

1475
1476

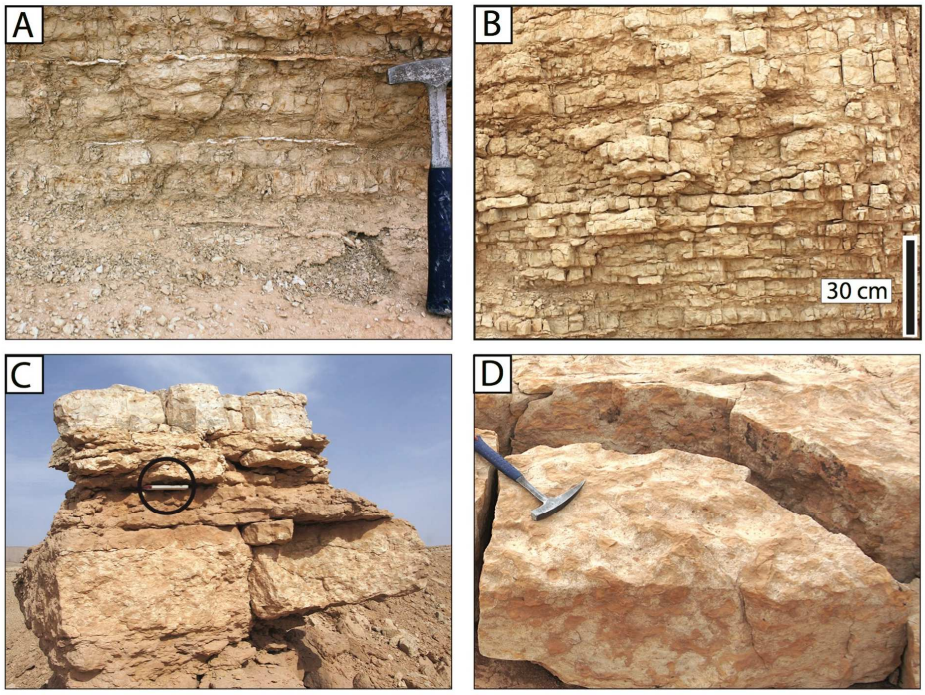

Figure 7

1477

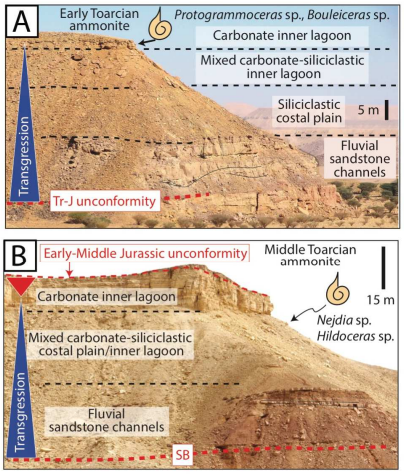

Figure 8

1478

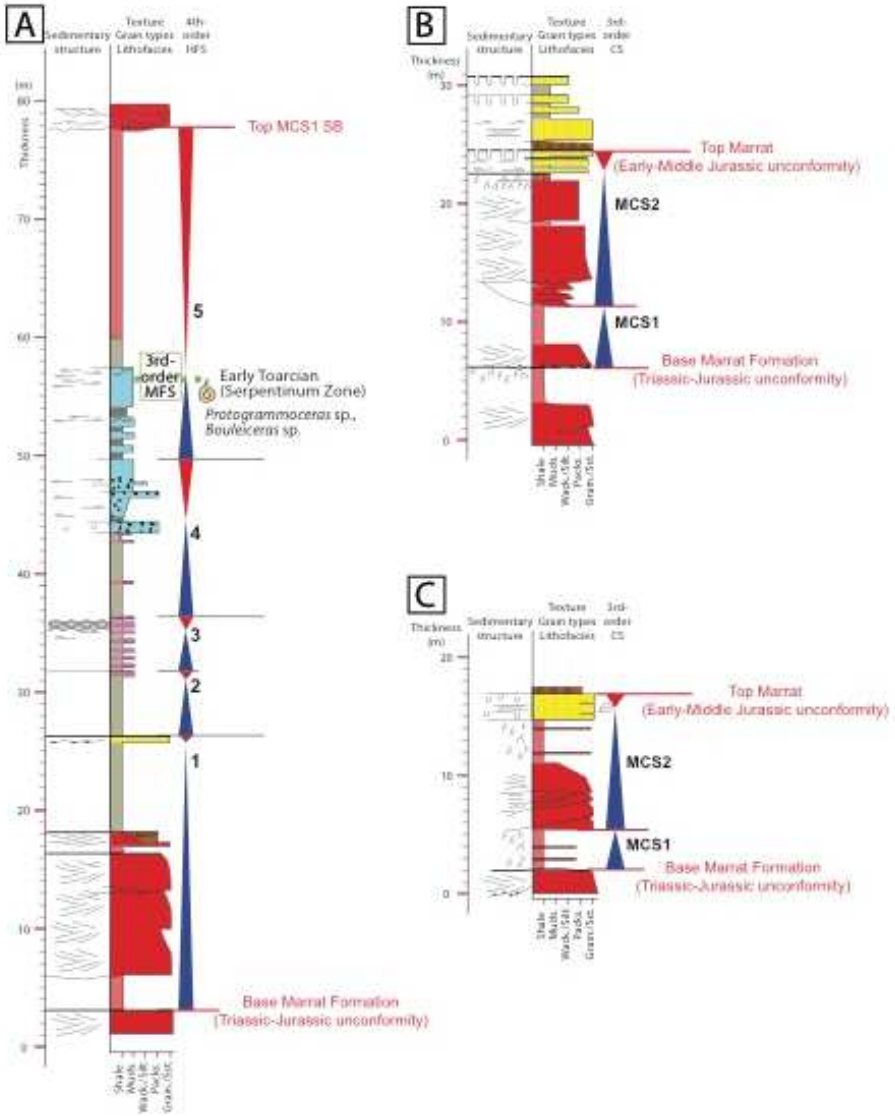

Figure 9

1479

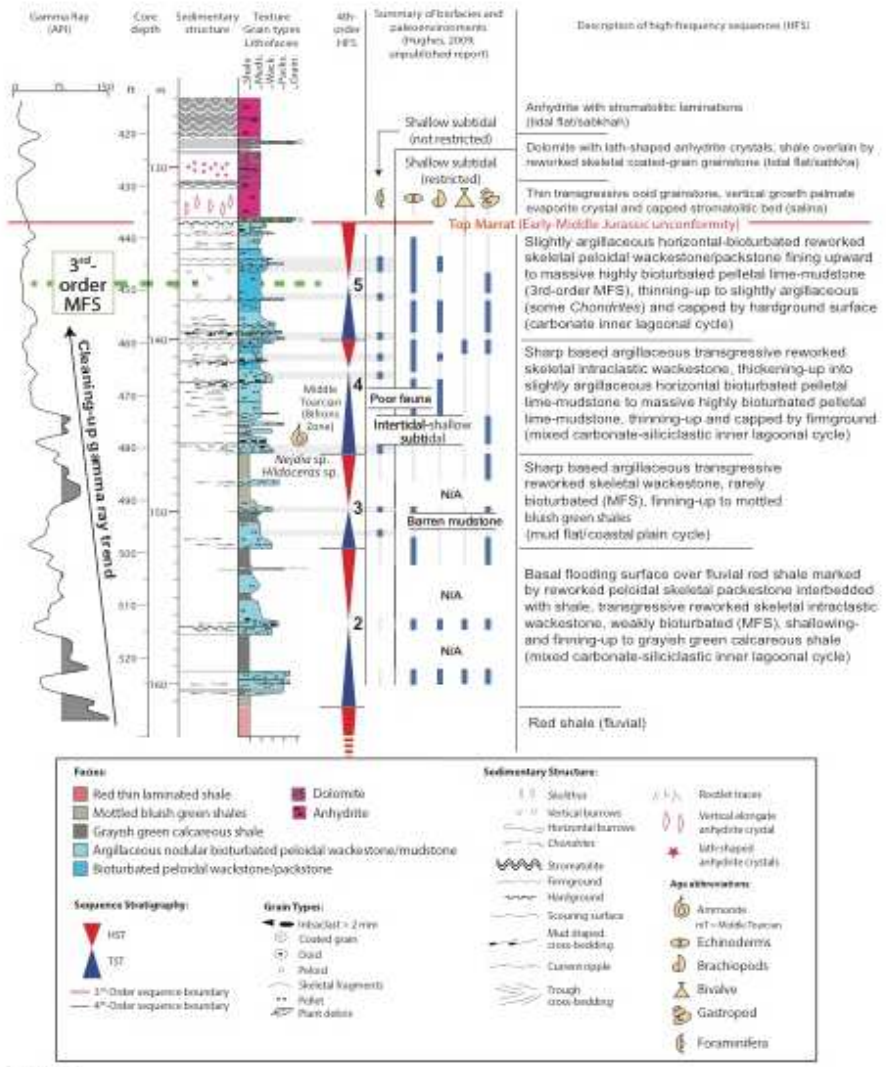

Figure 10

1480

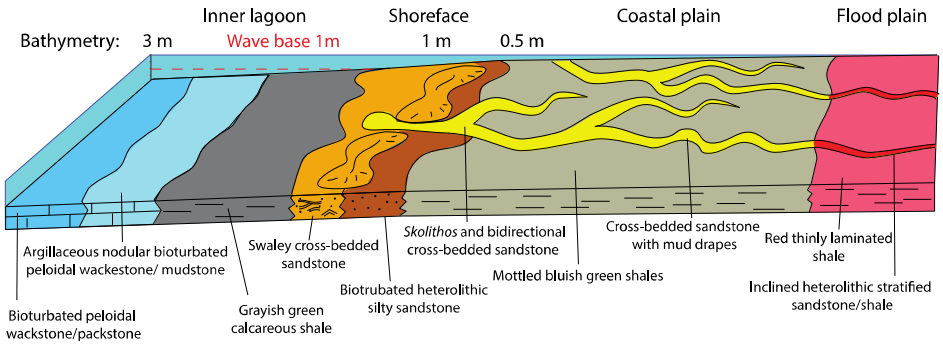

Figure 11

1481

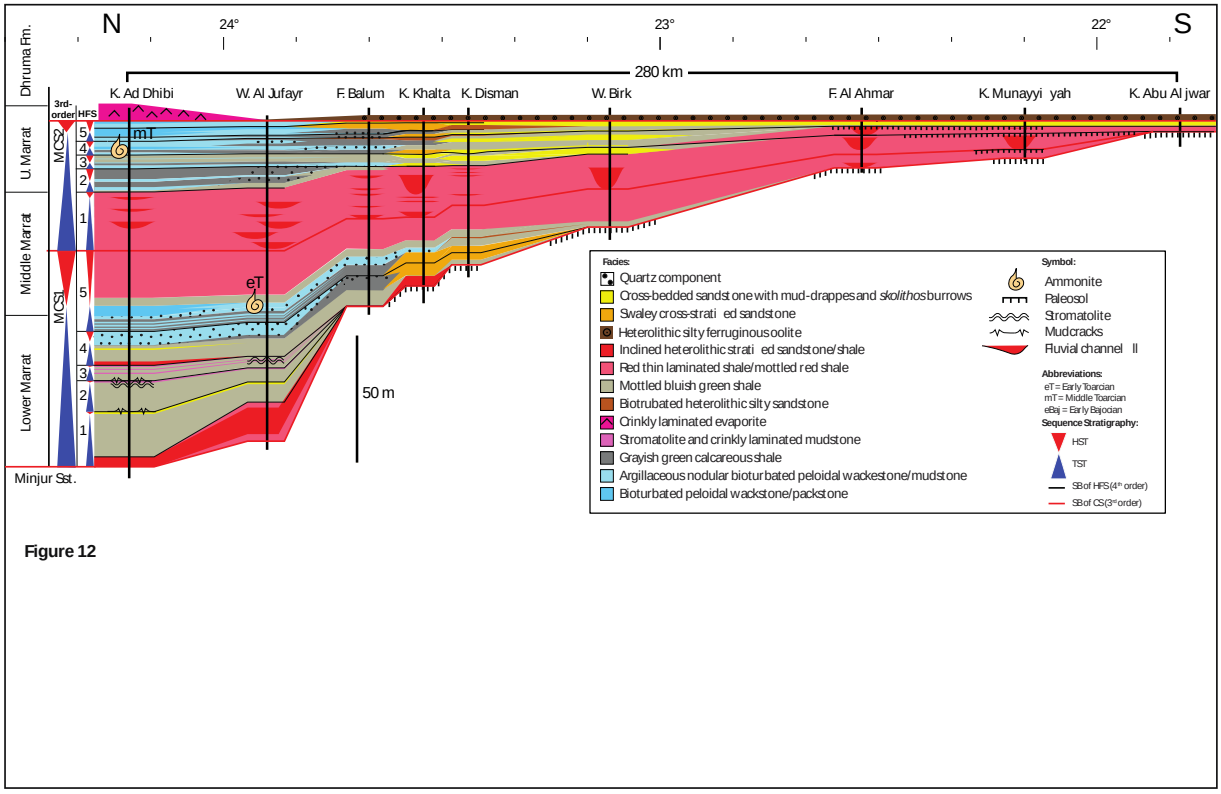
N
24°
23°
22°
S
280 km
Dhruma Fm.
U. Marrat
Middle Marrat
Lower Marrat
K. Ad Dhibi
W. Al Jufayr
F. Balum
K. Khalta
K. Disman
W. Birk
F. Al Ahmar
K. Munayyi yah
K. Abu Al jwar
3rd-order HFS
MCS2
MCS1
mT
eT
50 m
Minjur Sst.
Facies:
Quartz component
Cross-bedded sandstone with mud-drapes and skolithos burrows
Swaley cross-strati ed sandstone
Heterolithic silty ferruginous oolite
Inclined heterolithic strati ed sandstone/shale
Red thin laminated shale/mottled red shale
Mottled bluish green shale
Biotrubated heterolithic silty sandstone
Crinkly laminated evaporite
Stromatolite and crinkly laminated mudstone
Grayish green calcareous shale
Argillaceous nodular bioturbated peloidal wackestone/mudstone
Bioturbated peloidal wackstone/packstone
Symbol:
Ammonite
Paleosol
Stromatolite
Mudcracks
Fluvial channel II
Abbreviations:
eT = Early Toarcian
mT = Middle Toarcian
eBaj = Early Bajocian
Sequence Stratigraphy:
HST
TST
SB of HFS (4th order)
SB of CS (3rd order)

Figure 12

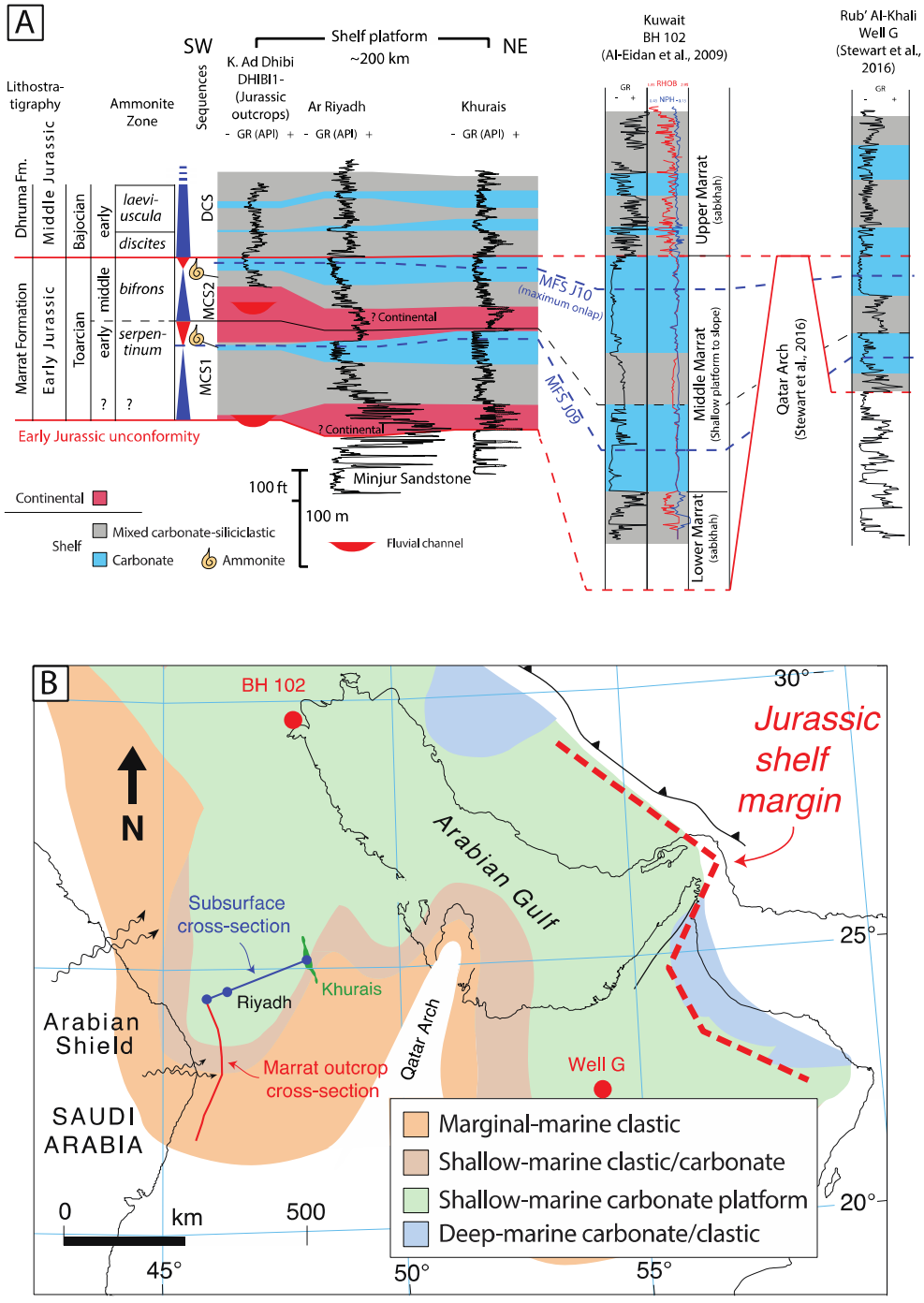

Figure 13

1483
1484

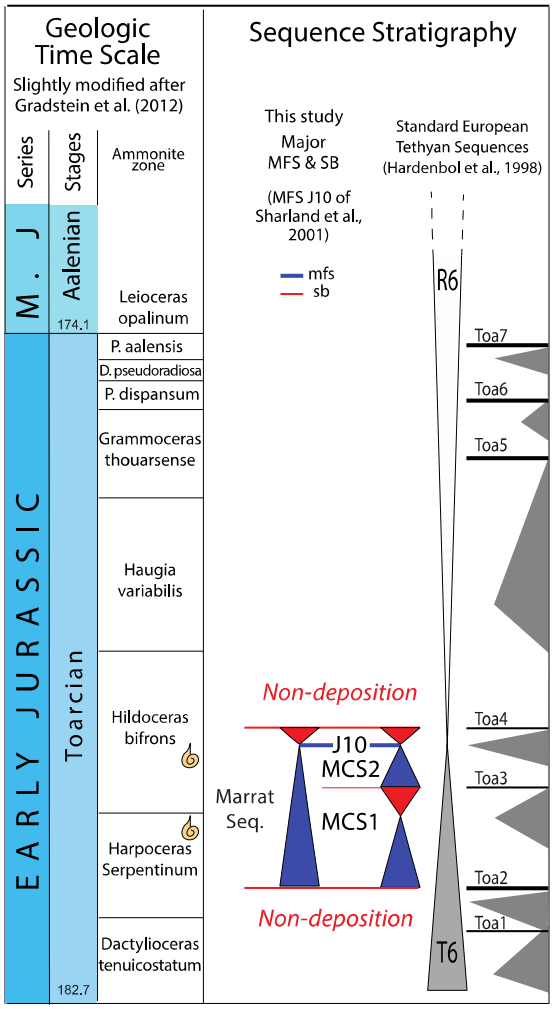

Figure 14

1485

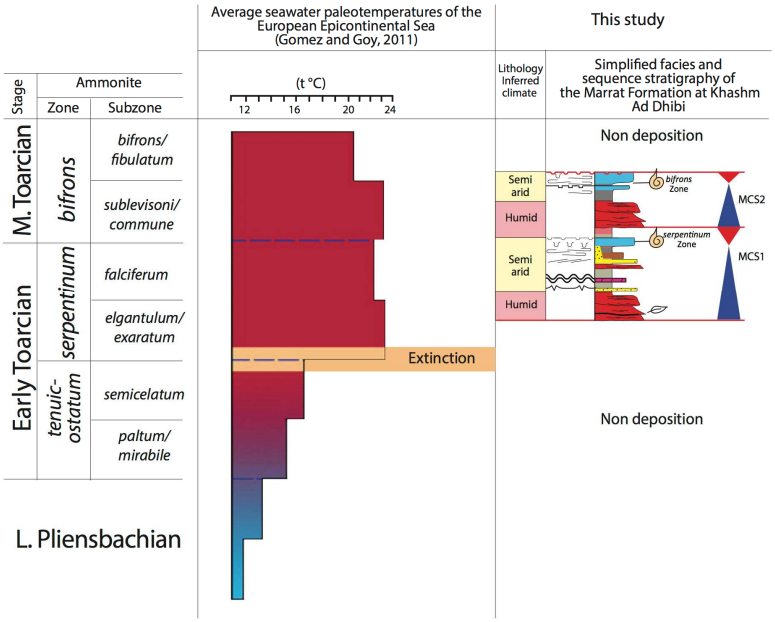

Figure 15

1486